

pubs.acs.org/acscatalysis Perspective

# Nontraditional Catalyst Supports in Surface Organometallic Chemistry

Ryan J. Witzke, Alon Chapovetsky, Matthew P. Conley,\* David M. Kaphan,\* and Massimiliano Delferro\*



Cite This: ACS Catal. 2020, 10, 11822-11840

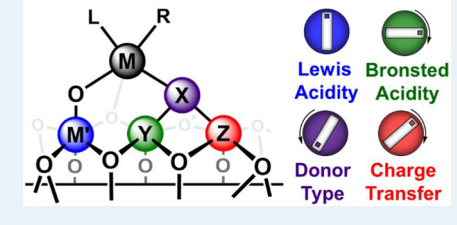


**ACCESS** 

III Metrics & More

Article Recommendations

ABSTRACT: The field of Surface Organometallic Chemistry (SOMC) aims to blend the positive attributes of homogeneous and heterogeneous catalysis. Significant insight into heterogeneous systems has been gained over the years through the synthesis, characterization, and application of well-defined surface organometallic catalysts, predominantly supported on silica and alumina. Considerable research efforts have focused on the application of homogeneous methods to the synthesis and characterization of these systems. Homogeneous catalysis has thrived on its ability to electronically and sterically tune ligands to yield desired reactivity and selectivity. Efforts



in SOMC, however, have only recently turned to harnessing the stereoelectronic diversity of potential inorganic support materials beyond silica and alumina in order to exert similar control on the reactivity of the organometallic active site. The support material is intrinsically linked to electronic structure and reactivity of heterogeneous organometallic systems in the same way that ligands exert control over homogeneous catalyst systems. The ability to tune the reactivity of heterogeneous catalysts by changing the support is of great value, and it is anticipated that this will represent an area of significant growth in the field. In this Perspective, the use and future of nontraditional catalyst supports, such as sulfated metal oxides, modified silicas, and redox active supports are discussed.

KEYWORDS: surface organometallic chemistry, heterogeneous catalysis, sulfated metal oxides, noninnocent ligands, catalysis

#### 1. INTRODUCTION

Catalysis plays a vital role in major sectors of the world's economy, such as petroleum (oil and gas), energy production, synthesis of fine chemicals, polymers, and the food industry. Together, these industries account for more than \$10 trillion of the world's gross domestic product (GDP). It is estimated that catalysis is responsible for 35% of global GDP, with the largest contribution coming from the production of fuels (e.g., gasoline, diesel, H<sub>2</sub>). The catalyst market alone is projected to have an approximate value of \$35 billion by 2025, and heterogeneous catalysts dominate this marketplace in large part because of their simple separation and recyclability. Continuous design and improvement are necessary to produce more active, selective, and stable catalysts.

Catalysts are divided into homogeneous catalysts, which are soluble in the reaction medium, and heterogeneous catalysts, which remain in the solid state. A heterogeneous catalyst typically consists of an active component (e.g., metal nanoparticles), promoters (e.g., tin, zinc, gallium, boron), and an inorganic inert, high-surface-area support material (e.g., metal oxides or chlorides, amorphous carbon). Silica (SiO) $_{22}$  alumina (Al $_2$ O $_3$ ), and magnesium chloride (MgCl $_2$ ) are the common support materials in industry, with silica being the most significant. Currently, ~80% of industrial processes rely on the use of heterogeneous catalysis, especially in the petrochemical and fine chemical industries. The widespread

application of supported catalysts in industry led to the development of numerous synthetic methods which enable their manufacture on a large scale; these methods are often complex and require several successive steps. The most common methods are<sup>2</sup> (1) homogeneous deposition-precipitation,<sup>3</sup> (2) impregnation,<sup>4</sup> and (3) thermal deposition.<sup>5,6</sup> These synthetic methods usually form ill-defined mixtures of active and dormant sites (e.g., different particle size, structure, and composition). Thus, understanding structure—reactivity relationships in these systems is complicated by uncertainties in the nature<sup>7</sup> and number<sup>8</sup> of catalytically active sites.

Surface organometallic chemistry (SOMC) has emerged as a new synthetic strategy for developing single-site, *homogeneous-in-function* heterogeneous catalysts. <sup>9,10</sup> This deposition method consists of the chemisorption of a well-defined, organometallic molecular fragment onto surfaces to yield an immobilized reactive organometallic species (Figure 1).

In many of these instances the homogeneous organometallic precursors exhibit far lower (or in some cases negligible or no)

Received: July 31, 2020
Revised: September 11, 2020
Published: September 14, 2020



Figure 1. Simplified depiction of a grafted organometallic complex.

catalytic activity in comparison with the supported species. 11,12 In addition, the inability of the supported organometallic species to undergo bi- or multimolecular degradation, 13,14 a common deactivation pathway in homogeneous catalysis, results in more persistent reactive catalytic species. Conversely, the limited stability of some organometallic species toward oxygen, water, and temperature is often sustained upon grafting to supports. This approach can also provide a nuanced understanding of active-site structures and catalytic mechanisms similar to that achieved in the study of homogeneous catalysts. The active sites are amenable to kinetic and spectroscopic characterization techniques, thereby providing opportunities for systematic investigation of the roles of the metal and the supporting ligand in the catalytic cycle. In this regard, advancement in spectroscopic techniques, such as solid-state dynamic nuclear polarization (DNP) nuclear magnetic resonance (NMR)<sup>15–18</sup> spectroscopy, X-ray absorption spectroscopy (XAS), <sup>19–22</sup> and periodic and cluster model calculations<sup>23</sup> has played a pivotal role in the progress of SOMC. Recent advances in predictive modeling of various spectroscopic signatures in well-defined catalysts represents a synergy between these two areas and enables previously inaccessible molecular level characterization of the supported organometallic fragments. 24-26 Pioneering works from the groups of Marks, 27-29 Basset, 30-32 Copéret, 33-35 Gates, 36-38 Tilley, 39-42 Scott, 43-45 and others 46-54 have demonstrated effective tuning of the activity and selectivity of single-site catalysts through precursor engineering and control over support platforms, harnessing fundamental structural and mechanistic insights into catalytic species for chemical processes which include polymerization/oligomerization, metathesis, hydrogenolysis, hydrogenation, dehydrogenation, and hydroelementations (Si, B). The bulk of this work focuses on grafting organometallic precursors onto amorphous dehydroxylated silica (and alumina), likely due to its facile synthesis, controlled surface hydroxyl concentration (200 °C density of Si-OH ~ 4.9 OH nm<sup>-2</sup>; 500 °C density of Si-OH  $\sim 1.8$  OH nm<sup>-2</sup>; 700 °C density of Si-OH  $\sim 0.9$  OH  $nm^{-2}$ ), 55,56 high surface area (50 to 1000  $m^2$   $g^{-1}$ ), and availability of different structures and morphologies (microporous: silica gel,<sup>57</sup> mesoporous: MCM41,<sup>58</sup> SBA15<sup>59</sup>).

Other materials and surfaces can also serve as supports for single-site organometallic catalysts. In this Perspective, we will describe examples of organometallics grafted onto underexplored supports, such as sulfated metal oxides, modified silicas, redox active supports, and others. The reader will recognize that some of these inorganic supports can function as both ancillary ligands and activators, reminiscent of noninnocent organic ligands in homogeneous catalysis. We envision that noninnocent inorganic supports will become increasingly important as the field of SOMC continues to progress,

enabling novel reactivity through stereoelectronic manipulation of the surface environment. We will emphasize future opportunities to advance SOMC and discover unprecedented catalytic reactivity for each class of support. When possible, we will draw parallels between the new supports and homogeneous catalysis and underlie elementary mechanisms and mechanistic motifs. Additionally, we foresee that advanced spectroscopy and imaging tools, coupled with data science and computational efforts, will facilitate rigorous characterization of the structure and reactivity of supported organometallic fragments on nonclassical surfaces. The hope is that this integrated approach will ultimately bridge the gap between homogeneous and heterogeneous catalysis.

## 2. SULFATED METAL OXIDES (SMOS): A HETEROGENEOUS WEAKLY COORDINATING

Weakly coordinating anions  $^{64-66}$  are used in homogeneous catalysis to obtain electrophilic metal species. For example, perfluorinated phenyl borane and borates  $(B(C_6F_5)_3$  and  $[Ph_3C][B(C_6F_5)_4]$ , respectively) are used as cocatalyst/alkyl abstractor  $^{67}$  with Group 4 metallocenes to generate extremely active, electron-deficient, and coordinatively unsaturated olefin polymerization catalysts. While not metal based, frustrated Lewis pairs (FLPs) have analogous characteristics as weakly coordinating anions and their cationic metal counterparts. These properties allow FLPs to catalyze stereoselective hydrogenations.  $^{69,70}$ 

Translation of weakly coordinating anion characteristics and properties to heterogeneous systems has been a goal of many groups, especially toward catalysts for hydrogenation and polymerization reactions.  $^{71,72}$  High-surface-area sulfated metal oxides of alumina (SO<sub>4</sub>/Al<sub>2</sub>O<sub>3</sub>) and zirconia (SO<sub>4</sub>/ZrO<sub>2</sub>) are prepared by the high-temperature calcination of  $\rm H_2SO_4$ -doped parent oxides.  $^{73,74}$  DFT studies on periodic ZrO<sub>2</sub> models show that sulfuric acid dissociates on Zr–O–Zr bridges to form Brønsted acidic –OH groups on the surface.  $^{75}$  The Brønsted acid strength and nature of these sites is a topic of ongoing debate, having been originally characterized as "superacid" materials (more acidic than neat sulfuric acid), while more recent works dispute this characterization and attribute their reactivity to other factors, including strong oxidizing behavior.  $^{73,76-80}$ 

Both silica and SMOs react with organometallics through protonolysis of a M–R group by a Brønsted acid site (Figure 2). Reactivity and spectroscopic trends show that silica reacts to form  $\equiv\!\!\text{SiO}-ML_n$  type surface species (Figure 2a). In contrast, the more acidic SMOs tend to react with organometallics to form weakly associated [ML\_n][SMO] ion-pairs (Figure 2b). In many respects, the weak interaction between SMOs and the cationic metal complexes are analogous to homogeneous ion-paired transition metal polymerization catalysts  $^{67,81,82}$  and have been shown to afford similar results. (Figure 3). In addition to  $SO_4/Al_2O_3$  and  $SO_4/ZrO_2$ , SOMC has been used to synthesize organometallic complexes supported by sulfated Fe<sub>2</sub>O<sub>3</sub>, TiO<sub>2</sub>, and SnO<sub>2</sub>.  $^{83,84}$ 

The origin of these ion pairs is complex, but at least partially related to the difference in acidity of –OH groups on silica compared with –OH groups on SMOs. Though simplistic, this model is intuitively satisfying because acid strength is a key design element of weakly coordinating anions in solution and would be expected to translate to surface species. However,

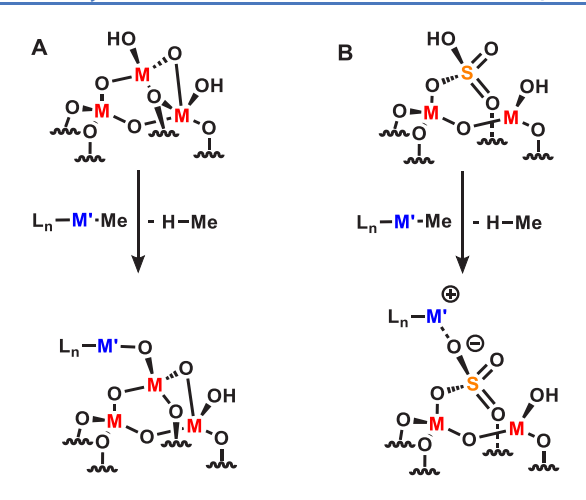


**Figure 2.** Grafting process and coordination mode for traditional oxide surfaces (A) and sulfated metal oxides (B). M = Si, Al, Zr, Ti, In, Ce; M' = Tansition metal; E = Tansition metal.

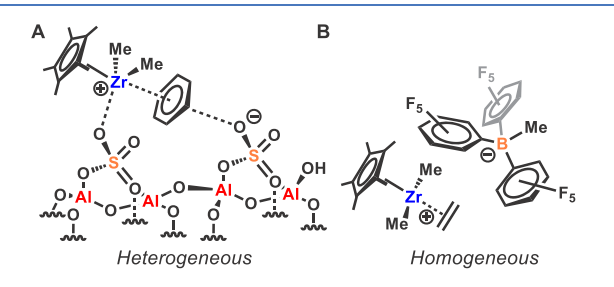


**Figure 3.** Structures depicting the activation of benzene (A) and ethylene (B) by the  $Cp*Zr(CH_3)_2^+$  cation stabilized by a sulfated alumina surface (A) and a methyl-tris(pentafluorophenyl)boryl anion in solution (B).

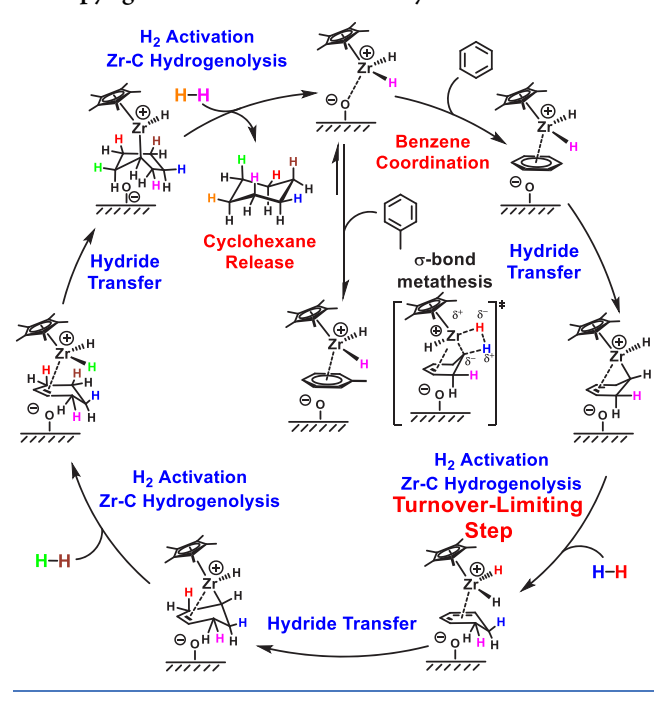
SMOs can react with organometallic complexes through mechanisms other than protonolysis (vide infra).<sup>86</sup>

A wide range of organometallics form well-defined ion-pairs sites on SMOs. Grafting  $Cp_2ZrMe_2$ ,  $Cp*ZrMe_3$ ,  $Cp*ZrBn_3$  (Bn = benzyl), and  $Cp*ZrPh_3$  on  $SO_4/ZrO_2$  and  $SO_4/Al_2O_3$  resulted in materials capable of arene hydrogenation. S<sup>7,88</sup> <sup>13</sup>C CPMAS NMR and X-ray adsorption spectroscopy (XAS) studies are consistent with the formation of highly electrophilic  $d^0$  single-site catalysts. Compared with their sulfated alumina homologues,  $SO_4/ZrO_2$ -supported catalysts are an order of magnitude faster with respect to the hydrogenation of benzene. S<sup>88</sup>

The electrostatic interaction(s) of the cationic Zr complex with SO<sub>4</sub>/Al<sub>2</sub>O<sub>3</sub> is critical in arene hydrogenation reactions. The computed mechanism for Cp\*ZrH<sub>2</sub>+/SO<sub>4</sub>/Al<sub>2</sub>O<sub>3</sub>-mediated benzene hydrogenation is shown in Scheme 1. A key step is the coordination of benzene to the Cp\*ZrH<sub>2</sub>+ fragment, which occurs between the cationic Zr and anionic rate and is analogous to displacement of a weakly coordinating anion by substrate in early metal polymerization catalysts. <sup>67,81,82</sup> This coordination environment results in hydrogenation occurring on the arene face coordinated to Zr and can be used to rationalize high selectivity for benzene hydrogenation in mixtures of arenes including mesitylene, ethylbenzene, and toluene; <sup>88</sup> or to diastereoselectively access all *cis*- products from facially selective arene hydrogenation reactions.

Electrophilic organometallic sites generated on SMOs are also active in olefin polymerization reactions, which demonstrates the weakly coordinating nature of SMOs. Organo-

Scheme 1. Computed Catalytic Cycle for Cp\*ZrH<sub>2</sub>+/SO<sub>4</sub>/Al<sub>2</sub>O<sub>3</sub>-Mediated Benzene Hydrogenation. Reused from Ref <sup>87</sup>. Copyright 2013 National Academy of Sciences



zirconium complexes react through protonolysis with -OH groups on  $SO_4/Al_2O_3$  nanoparticles to form a cationic surface-bound organometallic fragment from  $^{13}C$  CPMAS NMR studies.  $^{90}$  ZrBn $_3/SO_4/Al_2O_3$  is a very active polymerization catalyst, and the reaction was found to be more efficient in heptane relative to toluene, suggesting that toluene inhibits formation of key Zr(R)(olefin) $^+$  intermediates under the reaction conditions. ZrBn $_3/SO_4/Al_2O_3$  incorporates 1-hexene at greater rates when copolymerized with ethylene than the Cp\*ZrMe $_2/SO_4/Al_2O_3$  system, a reflection of the lower coordinative saturation of the benzyl-supported catalyst.

Precatalysts for olefin polymerization containing late transition metal complexes also react with SO<sub>4</sub>/ZrO<sub>2</sub> to form well-defined active sites. The reaction of a  $(\alpha$ -diimine)NiMe<sub>2</sub> with  $SO_4/ZrO_2$  forms ( $\alpha$ -diimine)NiMe<sup>+</sup>/ $SO_4/ZrO_2$  that catalyzes the polymerization of ethylene with a TOF of 21000 h<sup>-1</sup> at 40 °C in toluene. <sup>48</sup> This catalyst also incorporates a small amount of methyl 10-undecenoate polar comonomers into polymer chains in copolymerization reactions. <sup>13</sup>C labeling studies suggest that all Ni-Me<sup>+</sup> sites in this material are active in polymerization reactions.<sup>48</sup> Pd  $\alpha$ -diimine complexes also graft onto SO<sub>4</sub>/ZrO<sub>2</sub> through protonolysis and copolymerize ethylene and methyl acrylate with up to 0.46% incorporation.<sup>91</sup> However, this catalyst contains only ∼9% active Pd−Me<sup>+</sup> sites and is less active than the homogeneous analogues Pd complexes with fluorinated aryl borate anions for the incorporation of methyl acrylate (up to 12%) into polyethylene chains.92

The electrophilic  $Cp^*(PMe_3)IrMe^+$  organometallic fragment, a canonical early example of C–H bond activation studied in detail in solution, represents a compelling probe for the electronic interaction between the surface and supported organometallic complex because of the strong dependence between activity and  $Ir-O_X$  ( $O_X$  = surface oxygen) covalency.  $Cp^*(PMe_3)IrMe^+$  grafted on  $SO_4/ZrO_2$  catalyzes H/D exchange reactions of methane and arenes at

Figure 4. Observation of anomalous Cp\* deuteration during the chemisorption of Cp\*(PMe<sub>3</sub>)IrMe<sub>2</sub> onto sulfated surfaces and proposed operant redox mechanism involving surface pyrosulfate groups.

room temperature,  $^{46,47}$  whereas the analogous silica-supported Ir complex is essentially inactive under these reaction conditions. This system is also shown to recapitulate the stoichiometric reactivity of the homogeneous cationic iridium complex in a number of reactions including aldehyde decarbonylation and the formation of the Ir(V) trihydride in the presence of dihydrogen. These results underscore the potential of the  $SO_4/ZrO_2$  support in facilitating the formation of an electrophilic reactive metal center that is not possible on traditional inorganic scaffolds such as silica.

Imbuing electrophilic character to an organometallic iridium center was extended to enable catalytic olefin hydrogenation and stoichiometric alkane dehydrogenation upon supporting  $(^{dm}Phebox)Ir(OAc)_2$  on  $SO_4/ZrO_2$   $(^{dm}Phebox) = 2,6-bis(4,4-bis)$ dimethyloxazolinyl)-3,5-dimethylphenyl). 47 (dmPhebox)Ir-(OAc)<sub>2</sub>/SO<sub>4</sub>/ZrO<sub>2</sub> mediates stoichiometric dehydrogenation of nonane at 120 °C, which forms an iridium hydride on the surface. The molecular iridium diacetate requires 200 °C to achieve appreciable conversion of in nonane dehydrogenation. Computational interrogation of this process suggested that the rate limiting transition state for dehydrogenation was lowered by 5.1 kcal/mol for the complex on the sulfated surface, and that the slow elementary step in this process is  $\beta$ -hydride elimination, consistent with previous observations for the molecular system. 96 Interestingly, the noncoordinating nature of the surface facilitates desorption after the addition of an exogenous coordinating X-type ligand, such as tetrabutylammonium acetate, which enables characterization of intermediates by solution NMR spectroscopy. The SO<sub>4</sub>/ZrO<sub>2</sub>-supported complex was also an efficient catalyst for olefin hydrogenation, effecting greater than 20 000 turnovers in the hydrogenation of propene at 120 °C after 52 h on stream. The molecular complex supported on silica was found to be inactive under these conditions.

While the noncoordinating nature of the sulfated oxide surface has been reliably translated into enhanced reactivity in a number of organometallic catalytic systems as detailed above, the reactivity of these surfaces is not limited to Brønsted acidity. SMOs can also act as strong oxidants, and oxidative sites on SMOs are invoked in mechanistic proposals for key steps in  $SO_4/ZrO_2$ -catalyzed alkane isomerization. The

redox activity of these sulfated surfaces toward organometallic complexes was first observed as a side reaction in the chemisorption of Cp\*(PMe<sub>3</sub>)IrMe<sub>2</sub> (Figure 4). During grafting reactions, the excess in solution unexpectedly incorporates deuterium in Cp\*-Me groups. This occurs through reversible electron transfer from the Ir(III) complex to a highly electron deficient pyrosulfate group on the surface, followed by abstraction of a hydrogen atom to form the cationic tetramethylfulvene-Ir(III) cation on the surface. Computational investigation into the electron affinity of various candidate surface species found that the addition of an electron to a surface pyrosulfate structure was energetically favorable by 21.5 kcal/mol, whereas electron transfer to a representative electron deficient monosulfate structure was disfavored by 17.6 kcal/mol, strongly supporting the surface pyrosulfate as the identity of the redox active moiety. The relative surface coverage of strong Brønsted acid sites and redox active sites could be modulated as a function of sulfate loading (consistent with the redox activity of the aggregated pyrosulfate) and surface hydration. Dehydrating conditions are required to form the oxidizing pyrosulfate, and chemisorption of water is required to generate strong Brønsted acidic sites. The electron transfer in this system ultimately results in isotopic labeling of the organometallic precursor through a reversible oxidative grafting event and is not translated into a catalytic transformation; however, the observation of this redox interaction does open intriguing questions of whether or not the redox activity of the sulfated oxides can be leveraged as a redox noninnocent functionality to enable a productive catalytic process. For more on the potential application of redox active oxide surfaces in SOMC, see Section 5.

This discussion shows that SMOs are an example of supportdirected reactivity, and this work underscores the importance of the metal—support electronic interaction in controlling supported organometallic reactivity. These examples demonstrate the reliable generation of electrophilic active sites with reactivity similar to complexes with weakly coordinating counterions in solution. The complex chemical landscape of surface sulfate speciation can lead to significant differences in reactivity as a function of sulfate loading, calcination temperature, and dehydroxylation conditions. However, careful

Figure 5. Reaction schemes depicting the grafting of  $W(CH_2^tBu)_3(C^tBu)$  onto  $[N,O]SiO_2$  (A) and the W- $[N,O]SiO_2$  catalyzed metathesis of propane into other hydrocarbons (B).

preparation of the SMO surface to generate uniform Brønsted acid sites affords a valuable platform for heterogeneous electrophilic organometallic catalysis. This class of material and other Brønsted acidic modified oxides such as borated, phosphated, and tungstated zirconia and other oxides are expected to be increasingly leveraged in SOMC in years to come. 97,98

#### 3. MODIFIED SILICA SUPPORTS

Just as there are reactions that require electron-rich or -poor metal centers in homogeneous catalysis, tuning the electronic environment of an active site in a heterogeneous catalyst can affect catalytic rates and selectivity. While silica is particularly effective as an inert high surface area support to achieve site isolation of reactive catalytic species, the lack of variety in its electronic characteristics is a limitation for efforts in SOMC that rely on it exclusively as a medium for heterogenization. Synthetic efforts to modify surface functionalities on silica 100 and modulate its properties are analogous to organic ligand modification in homogeneous catalysis. Below we discuss the effects of substituting —OH groups on silica with —NH<sub>2</sub> groups, or activation of surface silanols with Lewis acids.

**3.1. Ammonia-Treated Silica.** As discussed above, silica is the most prevalent support material for SOMC. Some recent efforts have built upon that base knowledge to leverage the well-studied surface chemistry of silica to generate new stereoelectronically diversified catalytic environments through surface modification. Treatment of partially dehydroxylated SBA-15 with a flow of ammonia at 500 °C forms mostly  $\equiv$ Si-NH<sub>2</sub> surface species and a small amount of geminal silanols  $(=\text{Si}(\text{OH})_2)$ . Silica treated at 1100 °C  $(\text{SiO}_{2-1100})$  contains a very low surface coverage of  $\equiv$ Si-OH as well as strained siloxane bridges  $(\equiv$ Si-O-Si $\equiv$ ). Adsorption of ammonia at 200 °C  $(\text{NH}_3/\text{SiO}_{2-1100})$  results in opening of siloxane bridges to  $\equiv$ Si-OH and  $\equiv$ Si-NH<sub>2</sub> sites, some of which are close in space from solid-state NMR spectroscopy.

The surface N-donor ligands draw direct comparisons to homogeneous ligands featuring amine functional groups and are well suited for grafting of organometallic species. For example, the reaction of  $\mathrm{NH_3/SiO_{2-1100}}$  with  $\mathrm{Zr}(\mathrm{CH_2}^t\mathrm{Bu})_4$  yields either ( $\equiv$ Si-NH) $_2\mathrm{Zr}(\mathrm{CH_2}^t\mathrm{Bu})_2$  or ( $\equiv$ Si-NH)( $\equiv$ Si-O)Zr( $\mathrm{CH_2}^t\mathrm{Bu})_2$ . The corresponding Zr hydride species (isolated via treatment with hydrogen) catalyzes hydrogenolysis of butane to methane and ethane. Very subject to C'Bu)( $\mathrm{CH_2}^t\mathrm{Bu}$ ) are acts with  $\mathrm{NH_3/SiO_{2-1100}}$  to form a mixture of  $\equiv$ Si-O-W( $\equiv$ C'Bu)( $\mathrm{CH_2}^t\mathrm{Bu}$ )2 and ( $\equiv$ Si-NH)( $\equiv$ Si-O)W( $\equiv$ CH'Bu)2( $\mathrm{CH_2}^t\mathrm{Bu}$ ) (W-[N,O]-SiO2; Figure 5).

DFT studies determined that in the absence of the Si-NH<sub>2</sub> group the equilibrium favors the neopentyl/neopentylidyne structure over the bis(neopentylidene) structure. This is consistent with the observation of only the neopentyl/neopentylidyne structure upon grafting W( $\equiv$ C<sup>t</sup>Bu)(CH<sub>2</sub><sup>t</sup>Bu)<sub>3</sub> on silica. The presence of the Si-NH<sub>2</sub> moiety enables the  $\alpha$ -H exchange from a neopentyl ligand to the neopentylidyne ligand, thereby forming the bis(neopentylidene). W-[N,O]-SiO<sub>2</sub> catalyzes propane metathesis through the formation of a bis(neopentylidene) complex, which is facilitated by a nearby Si-NH<sub>2</sub> moiety. This is consistent with the silica-supported neopentylidyne complex's lack of reactivity with propane. 107

This support may have practical applications in studies of homogeneous systems that contains hemilabile ligands.  $^{108}$  The Si-NH $_2$  fragment in this system enables transformations at the metal center and can also dissociate to accommodate different coordination spheres. Additionally, incorporation of a more basic ligand on the surface could lead to stronger coordination and more electron-rich metal centers.

**3.2. Lewis Acid-Modified Silica.** Chemisorption of Lewis acids onto silica forms adducts with silanols to form strong Brønsted acid sites, or induces complex reorganization to form mixtures of strong Brønsted and strong Lewis sites. <sup>109,110</sup> This concept is closely related to acidic bridging silanols in zeolites (Figure 6a) and Lewis acid activated Brønsted acids that have found extensive utility in organic synthesis (Figure 6b). <sup>111</sup> Studies by Walzer <sup>112</sup> and Basset <sup>113</sup> showed that  $B(C_6F_5)_3$  reacts with partially dehydroxylated silica in the presence of amines to form  $[R_3NH][(C_6F_5)_3B\text{-OSi}\equiv]$  that react with zirconocenes to from cationic metallocene species active in polymerization reactions (Figure 6c). Scott showed that  $H_2O*B(C_6F_5)_3$  reacts with silica through formation of  $(C_6F_5)_2BOH$  to form strong Lewis acid  $\equiv SiO-B(C_6F_5)_2$  sites on the silica surface (Figure 6c). <sup>114</sup>

PhF\*Al(OC(CF<sub>3</sub>)<sub>3</sub>)<sub>3</sub><sup>115</sup> reacts with silica to form stable bridging silanols ( $\equiv$ Si-OH-Al(OR<sup>F</sup>)<sub>3</sub>, R<sup>F</sup> = C(CF<sub>3</sub>)<sub>3</sub>, Figure 6c). This behavior is in contrast to the examples of B(C<sub>6</sub>F<sub>5</sub>)<sub>3</sub> discussed above because PhF\*Al(OC(CF<sub>3</sub>)<sub>3</sub>)<sub>3</sub> is a stronger Lewis acid than B(C<sub>6</sub>F<sub>5</sub>)<sub>3</sub>. DFT studies using small cluster models accurately reproduce key spectroscopic features of  $\equiv$ Si-OH-Al(OR<sup>F</sup>)<sub>3</sub> and gas phase acidity calculations show that the bridging silanol is significantly more acidic than silanols in zeolite cluster models and common strong acids (HCl, H<sub>2</sub>SO<sub>4</sub>, HSO<sub>3</sub>CF<sub>3</sub>).

The deposition of a submonolayer of  $Zn^{2+}$  onto silica increases the Brønsted acidity of nearby hydroxyl sites that are sufficiently acidic to react with  $(C_5H_4Me)PtMe_3$ , an organo-

**Figure 6.** An acidic bridging silanol (a); a representative Lewis acid activated Brønsted acid (b); reactions of partially dehydroxylated silica with Lewis acids (c).

metallic unreactive to native silica. This anchoring site stabilizes a discrete and persistent Pt<sup>4+</sup>—H species on the surface and allows for its preparation and characterization under relatively mild reaction conditions (Figure 7A), which is

Figure 7. Comparison of Zn modified silica-supported Pt species (A) and Lewis acid modified homogeneous Pt complex (B). The Pt/Zn-SiO<sub>2</sub> system was active toward the chemoselective hydrogenation of nitro-aromatics to anilines (C).

unusual because Pt is known to readily aggregate to form nanoparticles on silica. The  $Pt/Zn/SiO_2$  species is active in the hydrogenation of butenes and nitro-aromatics. The conversion of nitro-aromatics to anilines was performed with high chemoselectivity, avoiding hydrogenation of aldehyde, ester, cyano, and halogen substituents (Figure 7B).

In addition to allowing for site-isolated surface organometallic species, the Zn also changes the reactivity of the Pt species. Other systems with Pt nanoparticles on silica have shown that addition of Zn leads to higher turnover rates for

dehydrogenation catalysis likely due to the electronic modulation of the Pt center. Similar effects have been studied in the homogeneous literature with the use of Lewis acid triggers. In these systems, remote binding of a Lewis acid to the ligand framework has been shown to modulate the reactivity of the transition metal (Figure 7C). Specifically, the binding of  $B(C_6F_5)_3$  at remote nitrogen positions of the pyrazine ligand leads to an increase in electrophilicity at the Pt, which then led to a 64 000-fold rate acceleration for biaryl reductive elimination.

Future work for this support should delve into the electronic effects of Zn and other Lewis acid additives to silica. One area of interest could be methane activation via supported Pt complexes. It has been shown that electrophilic homogeneous Pt complexes activate methane C–H bonds. 125,126 Grafting these systems to a Zn-modified silica could result in analogous rate increases to C–H activation for the new supported catalysts.

### 4. SURFACE PARAMETRIZATION OF NONTRADITIONAL SUPPORTS IN SOMC

Factors controlling the formation of covalently bound  $\equiv$ EO–ML<sub>n</sub> or [ML<sub>n</sub>][OE $\equiv$ ] ion-pairs shown in Figure 2 in well-defined surface species have obvious implications in catalysis. Organometallic Ir(III) complexes activate C–H bonds and are catalysts for H/D exchange reactions. Surface Cp\*IrMe-(PMe<sub>3</sub>)/oxide analogues are accessible from the reaction of Cp\*IrMe<sub>2</sub>(PMe<sub>3</sub>) and –OH sites on partially dehydroxylated silica, alumina, zirconia, B<sub>2</sub>O<sub>3</sub>/ZrO<sub>2</sub>, and SO<sub>4</sub>/ZrO<sub>2</sub> (Figure 8). Well-defined iridium sites are formed in these materials,

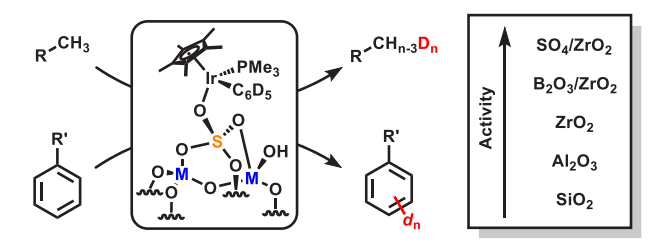


**Figure 8.** H/D exchange of arenes and alkanes catalyzed by supported Cp\*IrMe(PMe<sub>3</sub>) on a variety of oxides.

and  $[Cp*IrMe(PMe_3)]^+/SO_4/ZrO_2$  is highly active in H/D exchange of unactivated C-H bonds.  $Cp*IrMe(PMe_3)/SiO_2$  is essentially inactive in this reaction;  $Cp*IrMe(PMe_3)/Al_2O_3$  and  $Cp*IrMe(PMe_3)/ZrO_2$ , show moderate reactivity, and  $[Cp*IrMe(PMe_3)]^+/B_2O_3/ZrO_2$  exhibits increasing H/D exchange activity although still well below that of  $[Cp*IrMe(PMe_3)]^+/SO_4/ZrO_2$ . This activity trend reflects the formation of  $[Cp*IrMe(PMe_3)]^+$  on the ion-doped supports, which opens a coordination site at iridium to activate substrate in the H/D exchange reaction. This is not possible in the silicasupported sample because  $\equiv SiO-Ir(Cp*)(Me)(PMe_3)$  does not form an ion-pair under the reaction conditions.

A related argument that can explain the H/D reactivity trends in this class of catalysts is the difference in acidity between boric acid and sulfuric acid, the mineral acids used to form  $B_2O_3/ZrO_2$  and  $SO_4/ZrO_2$ , respectivley. Sulfuric acid is significantly more acidic than boric acid, which would suggest that a weaker ion pair forms between  $Cp*IrMe(PMe_3)^+$  and  $SO_4/ZrO_2$  compared with  $Cp*IrMe(PMe_3)^+$  and  $B_2O_3/ZrO_2$ , and this explains the higher reactivity of the former catalyst in

H/D exchange reaction. This is intuitive because of the well-known effects of ion pairing in solution; anions (X<sup>-</sup>) form weaker ion-pairs as the conjugate acid (HX) becomes stronger.

Though intuitive, quantification of acid strength on solids is challenging. 127,128 A common methodology to determine solid acidity is to soak the material in an aromatic Hammett indicator then determine the protonation state of the indicator colorimetrically; however, this method can produce misleading results. 129 For example, SO<sub>4</sub>/ZrO<sub>2</sub> was claimed to be a superacid on the basis of the low-temperature activity of SO<sub>4</sub>/ ZrO<sub>2</sub> in isomerization of alkanes<sup>73</sup> and colorimetric studies with Hammett indicators.<sup>74</sup> This is inconsistent with DFT studies showing that SO<sub>4</sub>/ZrO<sub>2</sub> contains -OH sites slightly less acidic than gas phase H<sub>2</sub>SO<sub>4</sub>. Additionally, experimental studies have proven that SO<sub>4</sub>/ZrO<sub>2</sub> cannot protonate weakly basic small molecules. <sup>130,131</sup> Indeed, a systematic evaluation of the effects of (tBu)2ArP, where the para position of the Ar group contains substituents that donate or withdraw electron density, showed that SO<sub>4</sub>/ZrO<sub>2</sub> has fairly low affinity for these phosphines and that SO<sub>4</sub>/ZrO<sub>2</sub> does protonate p-nitroaniline in MeCN (p $K_a$ (anilinium) = 6.22 in CH<sub>3</sub>CN), which confirms the lack of superacidic -OH groups on SO<sub>4</sub>/ZrO<sub>2</sub>.

Solid-state NMR methods are valuable in determining how a surface will interact with a substrate in a grafting reaction. DNP enhanced <sup>17</sup>O{<sup>1</sup>H} windowed-proton-detected local field with quadrupolar Carr Purcell Meiboom Gill (wPDLF-QCPMG)<sup>132,133</sup> experiments measure the dipolar coupling constants (R<sub>DD</sub>) between <sup>17</sup>O and <sup>1</sup>H spins and give O-H bond distances with picometer resolution.  $^{134}$  Ca(H<sub>2</sub>PO<sub>4</sub>)<sub>2</sub> is inarguably more acidic than Ca(OH)<sub>2</sub>.  $^{17}$ O( $^{1}$ H) wPDLF-QCPMG measurements show that -OH groups in Ca- $(H_2PO_4)_2$  have  $R_{DD}$  of 15.1  $\pm$  0.2 kHz, corresponding to an O-H distance of 1.025  $\pm$  0.005 Å. The O-H bond distance in  $Ca(OH)_2$  is 1.006  $\pm$  0.002 Å ( $R_{DD}$  = 16.0  $\pm$  0.1 kHz), which is shorter than the O-H bonds in Ca(H<sub>2</sub>PO<sub>4</sub>)<sub>2</sub> as expected. The <sup>17</sup>O{<sup>1</sup>H} wPDLF-QCPMG NMR spectra of Zn<sup>2+</sup> modified silica, discussed above, show that the average O-H bond distance is 1.034 ± 0.007 Å, longer than the average O-H bond distance in unfunctionalized silica  $(1.022 \pm 0.006 \text{ Å})$ . 117 This result indicates that silanols in Zn<sup>2+</sup> modified silica are more acidic than those on unfunctionalized silica, consistent with reactivity trends and temperature programed desorption (TPD) measurements.

Adsorption of small molecule probes (pyridine, phosphines, phosphine oxides, etc.) and measurement of FTIR and/or NMR properties of the adsorbate is a common method to assess acidity on oxide surfaces. 135 However, the Lewis acid activated Brønsted acid in  $\equiv$ Si-OH-Al(OR<sup>F</sup>)<sub>3</sub> (Figure 6c) reacts with Lewis bases to form LB → Al(ORF)3 that desorb from the silica surface. 116 The reaction of ≡Si-OH-Al(ORF)<sub>3</sub> with allyltriisopropylsilane forms [iPr<sub>3</sub>Si]- $[(R^FO)_3Al-OSi\equiv]$  (Figure 9a). The <sup>29</sup>Si CPMAS NMR spectrum of [iPr<sub>3</sub>Si][(RFO)<sub>3</sub>Al−OSi≡] contains a signal at 70 ppm and is consistent with silylium-like 136 surface species. This signal is ~17 ppm downfield from <sup>i</sup>Pr<sub>3</sub>Si/SO<sub>4</sub>/ZrO<sub>2</sub>, <sup>137</sup> 53 ppm downfield from R<sub>3</sub>Si-functionalized zeolites, <sup>138</sup> and 57 ppm downfield from trimethylsiliyl functionalized silica. 139-141 This trend indicates that the  $[(R^FO)_3Al-OSi\equiv]$  surface anion is more weakly coordinating toward R<sub>3</sub>Si-fragments than SO<sub>4</sub>/ ZrO2, zeolites, or silica.

Figure 9b shows the <sup>29</sup>Si NMR chemical shift of oxides functionalized with silanes, which tracks closely with trends found for molecular R<sub>3</sub>Si-X and [R<sub>3</sub>Si][X]. As the R<sub>3</sub>Si-X

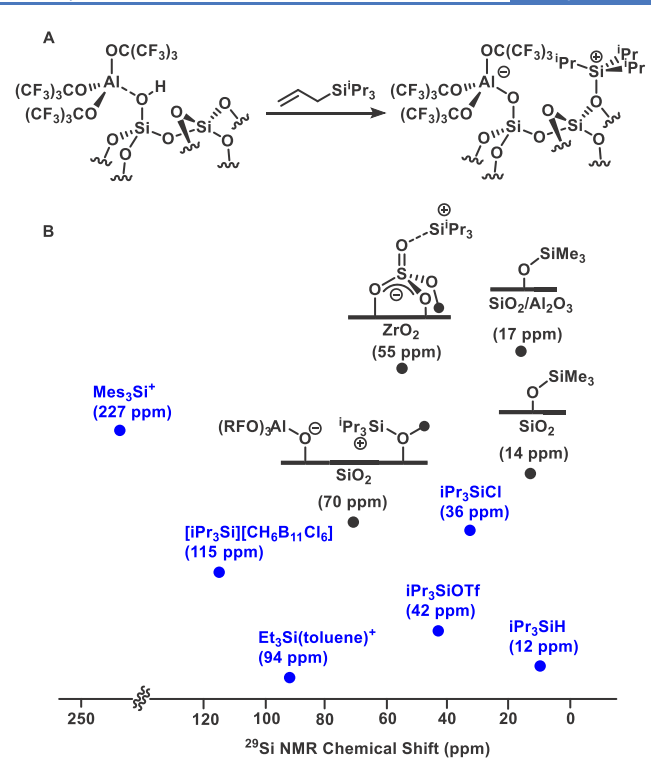


Figure 9. Generation of  $[^{i}Pr_{3}Si][(R^{F}O)_{3}Al-OSi\equiv]$  (a); a  $^{29}Si$  NMR chemical shift trend for  $R_{3}Si-oxides$ , selected  $R_{3}Si-X$  and selected  $[R_{3}Si][X]$  (b). Molecular  $R_{3}Si-X$  and  $[R_{3}Si][X]$  are shown in blue. Part b of figure adapted with permission from ref 142. Copyright 2020 The Royal Society of Chemistry.

approaches a free silylium ion, the <sup>29</sup>Si NMR chemical shift becomes more deshielded. This trend also tracks with ionpairing; [iPr<sub>3</sub>Si][CH<sub>6</sub>B<sub>11</sub>Cl<sub>6</sub>] has a significantly more deshielded <sup>29</sup>Si NMR chemical shift than <sup>i</sup>Pr<sub>3</sub>Si-OTf. This trend in deshielding is related to paramagnetic shielding of the <sup>29</sup>Si nucleus, which couples filled  $\sigma_{\rm SiC}$  bonding orbitals to the  $\sigma^*_{\rm SiX}$ antibonding orbital (or an empty p orbital in free R<sub>3</sub>Si<sup>+</sup>). The energy between these states decreases as R<sub>3</sub>Si-X approaches the free  $R_3Si^+$  cation, resulting in larger paramagnetic deshielding. This trend holds for the surface species as well. Paramagnetic deshielding increases, resulting in downfield <sup>29</sup>Si NMR chemical shifts, as the surface anion becomes more weakly coordinating. The <sup>29</sup>Si NMR chemical shift is an easy and practical probe to determine how R<sub>3</sub>Si-functionalized surfaces form ion-pairs, which could provide information about how to design surfaces more weakly coordinating than the  $[(R^FO)_3Al-OSi\equiv]$  surface anion.

#### 5. REDOX ACTIVE SUPPORTS

Industrially relevant processes are often catalyzed by nanoparticles supported on metal oxides. While in many cases the support acts simply as a high surface area dispersant for the reactive nanoparticles, an increasing appreciation for the role of the support as an active participant in catalysis has emerged in the recent literature. For example, ceria-supported rhodium and platinum systems are widely employed as three-way catalysts for automotive exhaust emission control. These systems perform (1) the reduction of NO to  $N_2$  (2) and the oxidation of CO to  $CO_2$  and (3) hydrocarbons to  $CO_2$  and  $H_2O$ . <sup>143</sup> Experimental and computational studies have shown that surface defect sites (steps and kinks) and oxygen vacancies

Table 1. State of the Art of Redox Active Supports Used for SOMC

Support	Metal Precursor	Structure on the Surface	Reaction Catalyzed
Titania (TiO2)	Rh(allyl) <sub>3</sub> 152,155	Rh And O TO T	C <sub>2</sub> H <sub>6</sub> Hydrogenolysis
	(CH <sub>3</sub> ) <sub>2</sub> Pt(COD) <sup>a</sup> 153		$ m H_2$ Evolution
	V(NMe <sub>2</sub> ) <sub>4</sub> <sup>154</sup>	NMe <sub>2</sub>	NA
	(CH <sub>3</sub> ) <sub>2</sub> Au(acac) <sup><i>b</i><sub>157</sub></sup>	Me Me	CO oxidation
	Cp₂Ni <sup>C</sup> 160		$ m H_2$ Evolution
	Cp₂Ru <sup>c</sup> 161	H H	$CO_2$ Reduction
Ceria (CeO <sub>2</sub> )	(CH <sub>3</sub> ) <sub>2</sub> Au(acac) <sup><i>b</i><sub>156</sub></sup>	Me Me	CO oxidation
$\mathrm{ITO}^d$	$[{\rm Ir}(L^*)(H_2O)_2(\mu\text{-}O)]_2^{\ell_{158}}$		Water oxidation
ІТО	(IMes)(COD)IrOH <sup>f159</sup>	OH OF STATE	Water oxidation

 $^{a}$ COD = 1,5-cyclooctadiene,  $^{b}$ acetyl acetone.  $^{c}$ Cp =  $C_{5}H_{5}$ ,  $^{d}$ ITO = Tin doped Indium Oxide,  $^{e}$ L\* = 2-(2'pyridyl)-2 propanolate,  $^{f}$ IMes = 1,3-Dimesitylimidazol-2-ylidene.

at the metal—support boundary participate in the catalytic process by stabilizing reactive intermediates and lowering the activation barriers for the three reactions. <sup>144,145</sup> A more subtle cooperation between the catalyst and the support is observed in cases of electronic metal support interactions (EMSI), a form of strong metal support interaction (SMSI). EMSI results from the dynamic interplay between the electronic structure of the metal oxide support and the supported catalyst. <sup>146,147</sup> In an early example of the recognition of this effect, Rodriguez and co-workers found that when comparing the transition states for the water splitting reaction across different catalysts, metal oxide-supported platinum nanoparticles were better at stabilizing reactive intermediates compared with bare platinum. <sup>148</sup> While this discrepancy can be partially rationalized by

the size and morphology of the Pt particles, charge transfer from the support to the active species also plays a major role in catalysis. UV photoelectron spectroscopy showed the supported systems exhibited a higher density of Pt 5d states for the supported platinum compared with the bare nanoparticles. Hence, the performance of the catalyst was related to the physical and chemical properties of the support. In another compelling example of EMSI between an oxide support and a metal nanoparticle, Saeys, Seebauer, and coworkers have shown that the ethylene hydrogenation performance of Pt on TiO<sub>2</sub> is strongly dependent on the carrier concentration of the support, which was inversely proportional to its size. Theoretical calculations by Verykios and coworkers have shown that the charge transfer capability of

titania drops from roughly 0.5 to 0.01 electrons (per support metal atom) when increasing the cluster size from 2.0 to 10 nm, consistent with the experimental trends. This phenomenon is referred to as the Schwab effect. While great progress has been made in the use of EMSI to enable catalytic activity and tune the performance of metal oxide-supported nanoparticles, leveraging this effect in SOMC has not been fully realized. Only a handful of examples of SOMC on redox active supports capable of EMSI have been reported, and electron transfer between the organometallic active site and support material has not been identified in these systems (Table 1). 152–161

TiO<sub>2</sub> is commonly used as a support for nanoparticle catalysts for a broad range of reactions. Its low cost, large carrier lifetimes, and tunable physical and electronic properties make it attractive for applications in electronics, catalysis, and photovoltaics.  $^{162-164}$  Additionally,  $TiO_2$  is an ideal support for traditional SOMC because of its high surface area (up to 400 m<sup>2</sup>g<sup>-1</sup>, depending on the synthesis and phase)<sup>165</sup> and the presence of Brønsted acidic hydroxyl groups on its surface. 166 Sato and co-workers have shown that Rh(allyl)<sub>3</sub> can be successfully grafted onto TiO2 at room temperature. 152 Addition of the rhodium precursor to partially dehydroxylated TiO<sub>2</sub> (pretreated under vacuum at 200 °C) resulted in the complete deposition of the organometallic species within 20 min. Partial characterization using FTIR and TPD were employed to confirm that each Rh metal was coordinated to one allyl ligand and two surface hydroxyl groups (in a bipodal fashion) (Figure 10A); however, further structural information

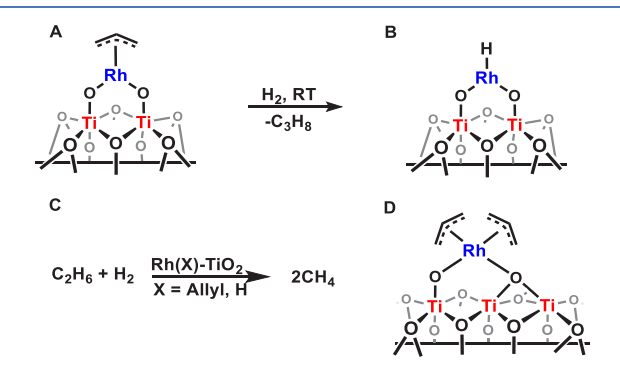


**Figure 10.** Structures of the allyl (A) and hydride (B) capped rhodium complexes on  $TiO_2$  and the hydrogenolysis reaction they catalyze as reported by Sato (C) and the diallyl rhodium complex on  $TiO_2$  (D) as prepared by Basset.

was not provided. The coordination environment and podality of the surface bound rhodium complex could be further confirmed via solid state H and C NMR measurements. Furthermore, given the dynamic electronic structure of titania, X-ray absorption, and photoelectron spectroscopies could elucidate the nature of electron transfer between the rhodium and the support. Treatment of the allyl capped complex with H<sub>2</sub> at room temperature results in the release of propane (1 equiv) and the formation of hydride species on the surface (Figure 10B). The same reduction at elevated temperatures (200° to 500°) forms rhodium nanoparticles. While all three were found to catalyze the hydrogenolysis of ethane, the allyl capped material was found to be more active than both the hydride and nanoparticle variants (Figure 10C).

Basset and co-workers also examined the structural implications of grafting Rh(allyl)3 onto a series of oxides including TiO2. 155 When comparing the kinetics of the reaction, it was found that the oxides reacted in the following order  $TiO_2 > SiO_2 > Al_2O_3 > MgO_1$  consistent with the increasing acidity of the hydroxyl groups on the surface of the support. 185,169 Upon addition of the Rh precursor to TiO2 (pretreated under vacuum at 250 °C), Rh(allyl)<sub>3</sub> releases a single equivalent of free propene, suggesting that the grafted Rh complex only forms a single Ti-O-Rh linkage. 15 reactivity was rationalized by the sparse hydroxyl surface coverage (~1 OH nm<sup>-2</sup>) on the titania surface. Subsequently, a stable 18 electron configuration could only be attained through binding to both a surface hydroxyl and a lattice oxygen (Ti-O-Ti) (Figure 10D). These findings were supported by FTIR measurements, DFT calculations, and previously reported EXAFS and TEM measurements. 169,170 The ability of TiO2 and other metal-oxides to bind to catalytically active organometallic precursors suggests that they can be employed as supports, while their dynamic electronic structure imparts them with broader reactivity, akin to redox noninnocent ligands in homogeneous catalysis.<sup>171</sup>

In most examples of SOMC, the support acts as an ancillary ligand that maintains a consistent electronic environment around the metal center. However, targeting support materials capable of EMSI, the role of the support can be expanded to actively play a part in the catalytic cycle, akin to a noninnocent ligand in homogeneous catalysis (Figure 11).61,172,173 Redox noninnocent ligands facilitate bond-making/breaking steps by reversible electron transfer to the catalyst during key steps throughout the catalytic cycle. 61 For example, work by Chirik and co-workers showed that iron and cobalt complexes stabilized by pyridine diimine pincer ligands catalyze multielectron transformations by reversibly storing one or more electrons in the  $\pi$ -system of the supporting ligand. <sup>174–177</sup> Similarly, conducting and semiconducting supports capable of EMSI could provide an orthogonal handle for modulating the activity of the grafted catalyst and unlocking new mechanisms of reactivity. Recent work by Basset and co-workers has shown that  $(CH_3)_2Pt(COD)$  (COD = 1,5-cyclooctadiene) can be chemisorbed onto high surface area, highly exposed, partially fluorinated (2.81 wt % F), {001} anatase titania under mild conditions (Figure 12). The resultant material was characterized using DRIFTS to confirm that the surface hydroxyl stretch (v OH at 3665 cm<sup>-1</sup>) disappears upon the addition of the organometallic precursor, suggesting that grafting occurs through protonolysis and the formation of a Ti-O-Pt bond.

Solid-state  $^{13}\text{C}$  NMR experiments on the free and supported platinum complexes were used to confirm that the methyl groups are lost from the platinum complex (as methane) upon grafting. XANES and EXAFS data, along with DFT calculations showed that platinum grafts to the surface in a bipodal fashion via a Pt–O–Ti linkage and a dative Pt–F  $\rightarrow$  Ti interaction with no change in the platinum oxidation state. Finally, unlike the bare  $\text{TiO}_2$ , the supported platinum complex was photoactive toward the hydrogen evolution reaction for up to 24 h.  $^{153}$  It was hypothesized that the migration of valence band electrons from the support to the surface was responsible for the hydrogen evolution activity.  $^{178,179}$ 

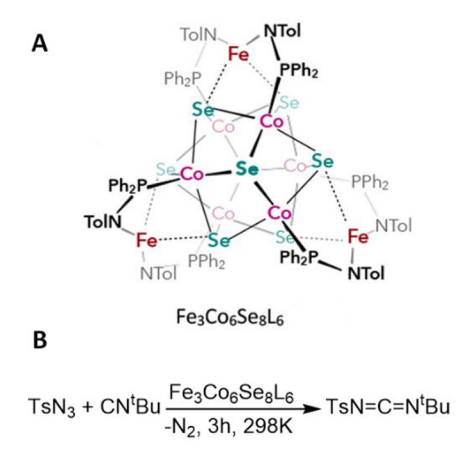
The EMSI in this example suggests that metal-oxides with tunable electronic properties can act as electron and hole reservoirs, storing and delivering multiple equivalents of

Figure 11. Reductive elimination of substrate R and R' from a metal (center) as governed by the electronics of the metal (left, top and bottom), ligand (top right), and support (bottom right).



Figure 12. Structure of  $(CH_3)_2Pt(COD)$  upon grafting to high surface area  $\{001\}TiO_2$ . Upon grafting, Pt maintains an oxidation state of 2+. The grafted platinum material was active toward the hydrogen evolution reaction.

electrons to a substrate with little to no kinetic barriers, and also function similarly to traditional supports by forming Ti-O-M linkages on the oxide surface. These physical properties are particularly exciting for applications toward difficult multielectron transformations, like water splitting or the reduction of  ${\rm CO_2}$  and  ${\rm N_2}.^{180-183}$  Lessons learned from the nanoparticle literature can guide future work with supported organometallics on redox active supports. The chemical and physical manipulation of conductive supports can evoke novel reactivity from the supported catalysts via EMSI and beyond. Perovskite-supported catalysts, for example, have been shown to catalyze the hydrogenation and dehydrogenation of small molecules (C2H6, N2, and CO2) through a hydrogen spillover mechanism reliant on the proton-conductive properties of the support. 184–186 In a more pertinent example to EMSI, electron transfer is governed by the properties of the support and can be optimized through the modification of its chemical properties. The introduction of dopants and defects can influence the charge transfer properties of the support. For example, the presence of iron, manganese, and other dopants has shown to modulate the charge transfer and subsequently catalytic activity of photoreduced TiO2 and CeO2. 49,187-191 Similarly, the introduction of oxygen and other defects on the surface has also been a useful strategy for augmenting the performance of single site catalysts on metal oxides. 192-195 The chemical and physical manipulation of redox noninnocent supports represents a new frontier in the field of supported organometallics and catalysis. Finally, there is an inverse relationship between the size of a support material and its electron transfer ability. Further utilization of this relationship results in the application of atomically precise nanoclusters as analogues for noninnocent surfaces. Small, 20-30 atom metal oxide or sulfide clusters represent robust synthons for the investigation of EMSI. 197-199 Their welldefined structures serve as controlled coordination environments for supported catalysts, while their solubility and physical properties make them amenable for investigations using a myriad of spectroscopic, magnetic, and electrochemical techniques, potentially allowing for rapid design iteration toward performance optimization. In recent work, Velian and co-workers prepared and characterized a series of well-defined nanopropellers of the form  $Fe_3Co_6Se_8L_6$  ( $L=Ph_2PNTol, Ph-phenyl, Tol=4-tolyl$ ) (Figure 13a). These nanoclusters consisted of a  $Co_6Se_8$  core that acts as a support for three iron complexes.



**Figure 13.** Schematic depicting the structure of the  $Fe_3Co_6Se_8L_6$  cluster (A) and the reaction scheme for the cluster catalyzed formation of tosyl carbodiimide from  $TsN_3$  and  $CN^tBU$  (B). Figure reprinted with permission from ref 200. Copyright 2019 American Chemical Society.

The cluster was chemically reduced and oxidized, and the resulting redox series was characterized using Mössbauer and UV—vis-NIR spectroscopies, along with cyclic voltammetry. Oxidation of the clusters led to the formation of reactive Fe species, while reduction occurred mostly on the inorganic support. These findings suggest that the redox active cluster could funnel electrons to a metal active site and bound substrate on the surface, drawing analogy to EMSI in extended redox active support systems. As a proof of concept, the clusters were shown to catalyze the reaction of TsN3 (Ts = Tosyl) and CN¹Bu to make TsNCN¹Bu (Figure 13B). The activity of the cluster was rationalized as the synergistic interaction between the chemically accessible iron complexes on the surface and the electron reservoir of the cluster support.

#### 6. ADDITIONAL SUPPORTS

**6.1. Magnesium Chloride** – **MgCl<sub>2</sub>.** Heterogeneous Ziegler–Natta catalysts account for a large fraction of polyethylene and polypropylene produced annually. <sup>203,204</sup> First-generation catalysts contained  $TiCl_4$  supported on  $MgCl_2$  with an alkyl aluminum cocatalyst. Later iterations contain Lewis bases and other electron donors that increase activity and selectivity of the polymerization. These catalysts are very active but usually produce polymers having very broad molecular weight distributions characteristic of "multi-site" polymerization catalysts. Information about the structure of the active site(s) in  $TiCl_4/MgCl_2/AlR_3$  is limited, but inference from extensive studies of organometallics in solution <sup>67</sup> suggests this catalyst contains a  $Ti^{IV}$ – $R^+$ .

The  $MgCl_2$  surface chemistry is complex.  $^{205-211}$  Studies of  $MgCl_2$  as alcohol solvates suggest that the specific ratio of alcohol to  $MgCl_2$  in the material results in different structures, which then affects activity and stereoselectivity in polymerization reactions.  $^{212-214}$  Internal donors, such as ethyl benzoate or phthalates, increase surface area of the  $MgCl_2$  support and may also coordinate directly to  $Ti.^{215-220}$  For e x a m p l e , s o l i d - s t a t e NMR s t u d i e s o f  $MgCl_2(THF)_{0.67}(TiCl_4)_{0.09}$  showed that THF coordinates to Ti. sites and ring opens to form Ti. alkoxy species.

This is an area in which the application of SOMC techniques could play a pivotal role in providing answers to understanding how organometallics interact with MgCl<sub>2</sub>. Cp\*<sub>2</sub>ThMe<sub>2</sub> reacts with anhydrous MgCl<sub>2</sub> through Lewis acid ligand abstraction to form Cp\*<sub>2</sub>ThMe<sup>+</sup> and MeMgCl<sub>n</sub><sup>-</sup> sites.<sup>222</sup> Approximately 50% of the Th–Me<sup>+</sup> sites are active in ethylene polymerization, with the reaction occurring exclusively at the Th-Me<sup>+</sup>. The chemistry of well-defined Ti organometallics with internal donors already coordinated to the metal could help elucidate their role in polymerization chemistry.

**6.2.** Magnesium Oxide (MgO). Magnesia is an ionic solid that contains mildly acidic surface —OH groups that can be used for grafting organometallic complexes in a fashion similar as silica. The MgO surface is generally considered to be significantly more Lewis basic in comparison to traditional supports such as silica and alumina. The surface of MgO has been studied by DFT calculations. These studies helped identify the experimental IR stretches and <sup>1</sup>H NMR resonances associated with surface hydroxyls in terms of local structure and coordination environment. Additionally, terminal and bridging hydroxyl groups have been identified by infrared spectroscopy. <sup>225</sup>

One major benefit of MgO as a support is the application of scanning transmission electron microscopy (STEM) for the determination of the surface coverage and size of grafted organometallic species (Figure 14).  $Ir(C_2H_4)_2(acac)$  (acac = acetylacetonate) grafts onto MgO by loss of acac and coordinates bipodally on MgO. The STEM images along with IR spectroscopy and EXAFS confirm the site isolation of the Ir complexes.

The grafted Ir complex catalyzes the hydrogenation of ethylene. A comparative study determined that MgO-supported species are less active in hydrogenation than more acidic zeolite or  $\gamma$ -alumina supports.

The electron-rich nature of MgO is an advantage when combined with  $Rh(C_2H_4)_2(acac)$ . After grafting and loss of acac, the dimeric Rh species catalyze the industrially important

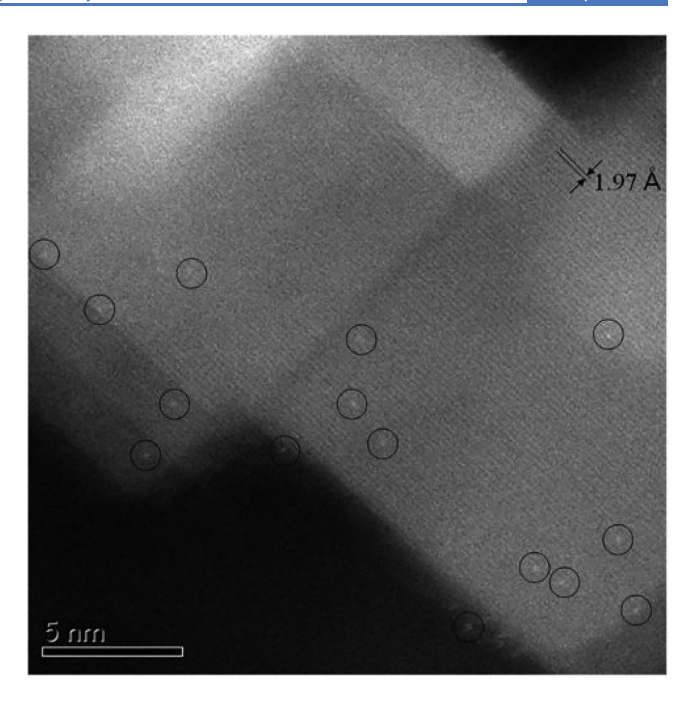


**Figure 14.** STEM image showing isolated Ir complexes on MgO crystallite. Reproduced with permission from ref 226. Copyright 2009 The Royal Society of Chemistry.

hydrogenation of 1,3-butadiene to butenes. After treatment with CO, the MgO-supported Rh dimers are significantly more selective than zeolite HY-supported catalysts. Other work has shown that MgO can support site-isolated Os catalysts for CO oxidation<sup>230</sup> and also Au catalysts for hydrogenation reactions.<sup>231</sup>

#### 7. OUTLOOK AND FUTURE DIRECTIONS

Surface organometallic catalysis combines the positive attributes of homogeneous catalysis with the chemical and physical properties of a heterogeneous system. The surface functional groups bound to the organometallic active site are generally spectator ligands to the specific catalytic elementary steps, but these groups do actively interact with and modulate the energetics of the active site frontier orbitals that are directly involved in catalytic transformations. In homogeneous catalysis, the role of the spectator ligand in enabling otherwise inaccessible modes of reactivity and in accelerating prohibitively slow elementary steps has long been recognized. Recent progress in the execution and interpretation of synthetic, spectroscopic, and computational techniques has led to the observation of similar relationships in the SOMC literature. However, increased understanding of synthetic techniques for the preparation of uniform sites on inorganic support materials, as well as the improvement in spectroscopic techniques and the correlation of these spectra to computational models of candidate surface structures will be required to define detailed structure function relationships in these systems. Advances in these areas have set the stage for a new phase in the expansion of this field, leveraging rationally designed catalyst-surface interactions to improve catalytic performance and enable previously inaccessible mechanistic pathways.

We anticipate that the areas highlighted in this Perspective will be explored and expanded, and new strategies for support mediated surface organometallic catalysis will be discovered. The application of highly Brønsted and/or Lewis acidic

inorganic materials to generate solid noncoordinating diffuse counterions after ligand abstraction was recognized relatively early in the SOMC literature as a method for the heterogenization of cationic olefin polymerization catalysts. Surfaces such as sulfated zirconia form weak ion-pairs analogous to the triflate anion. Lewis acid modified silicas are approaching the weak ion-pairs encountered with perfluorotetraphenylborate anions in homogeneous catalysis and show that strategies commonly employed in the generation of weakly coordinating anions in solution also apply to oxide surfaces. Future applications, beyond olefin polymerization and hydrogenation, may include olefin metathesis, <sup>232</sup>, <sup>233</sup> hydroelementations, <sup>234</sup>, <sup>235</sup> and cycloisomerization, <sup>236</sup> where the rate and/or selectivity of the catalyst is associated with the electrophilicity of the metal center. In order to improve these materials further, synthetic refinement will be necessary to generate well-defined and uniform active sites, particularly in the area of sulfated oxides, as these materials show unique complexity in surface speciation and active site structure. New supports based on strong Lewis acid materials may present an additional avenue of research. For example, aluminum trifluoride (AlF<sub>3</sub>) can be prepared as a high surface area  $(150-250 \text{ m}^2/\text{g})$  mesoporous material, and on the basis of computational and empirical ammonia and fluoride dissociation energies, it is comparable to SbF5 in Lewis acidity.237

Redox active inorganic support materials hold exceptional promise to play a synergistic role with surface organometallic catalysts. A support material with the appropriate redox potential could function as redox noninnocent ligands do in homogeneous catalysis. The strategic selection of metal oxides and dopants might produce supports with Fermi energies that will allow them to reversibly accommodate electrons over the course of the catalytic cycle. Furthermore, these supports could serve as electron reservoirs capable of delivering multiple reducing equivalents for multielectron transformations, such as N<sub>2</sub> and CO<sub>2</sub> reduction, with low kinetic barriers, obviating the need for iterative chemical reductions. Complex oxide materials such as perovskites offer an attractive option for future investigation of redox active materials because of the diverse range of candidate materials which provide access to a variety of bandgaps and Fermi levels. Furthermore, the band structure of some complex oxide materials can be continuously varied by dopant concentration and element substitution. 238,239

Surface organometallic catalysis beyond oxide supports also represents an area of great promise which is all but completely unexplored. Expanding beyond oxides to pnictogenides, halides, and other chalcogenides affords a wide range of opportunities to explore surface organometallic catalysis in a variety of coordination structures, bonding motifs, and electronic environments. One major challenge with the exploration of these materials is the synthesis of persistently high surface area morphologies with low oxygen contamination containing uniform surface coverage of reactive functional groups. Some progress has been made in the area of amine substituted silica as a support for organometallic catalysts (vide supra); however, these materials differ significantly in structure from the bulk nitride, and structural rearrangement to expose subsurface oxygen atoms remains a concern under reaction conditions. Nitride and phosphide materials, as well as the mixed oxynitride and oxyphosphide ternary compounds offer decreased bandgaps relative to their oxide analogues and thus

might represent additional candidates for redox active support materials. Increased donor strength and orbital overlap for these materials also may be a promising route to the stabilization of isolated late transition metal surface organometallic complexes and catalytic intermediates.

Decades of research have demonstrated that the immobilization of organometallic fragments on oxide supports is a powerful strategy for harnessing reactive species such as the canonical low coordinate early transition metal hydrides. 9,240 The nature of the organometallic fragment in SOMC has been extensively studied, with representative examples of nearly every transition metal having been explored. In contrast, relatively few inorganic support materials have been studied, despite the fact that the functional groups on the surface are inherently related to the reactivity of the supported organometallic complex. As the role of the support as a functional ancillary ligand continues to be developed and appreciated, a vast new chemical space will engender innovation in the field, and new frontiers in surface organometallic catalysis will emerge.

#### AUTHOR INFORMATION

#### **Corresponding Authors**

Matthew P. Conley – Department of Chemistry, University of California, Riverside, Riverside, California 92521, United States; orcid.org/0000-0001-8593-5814;

Email: matthew.conley@ucr.edu

David M. Kaphan — Chemical Sciences and Engineering
Division, Argonne National Laboratory, Lemont, Illinois 60439,
United States; orcid.org/0000-0001-5293-7784;
Email: kaphand@anl.gov

Massimiliano Delferro — Chemical Sciences and Engineering Division, Argonne National Laboratory, Lemont, Illinois 60439, United States; orcid.org/0000-0002-4443-165X; Email: delferro@anl.gov

#### **Authors**

Ryan J. Witzke — Chemical Sciences and Engineering Division, Argonne National Laboratory, Lemont, Illinois 60439, United States

Alon Chapovetsky — Chemical Sciences and Engineering Division, Argonne National Laboratory, Lemont, Illinois 60439, United States

Complete contact information is available at: https://pubs.acs.org/10.1021/acscatal.0c03350

#### **Author Contributions**

The manuscript was written through contributions of all authors. All authors have given approval to the final version of the manuscript.

#### **Funding**

This work was supported by the U.S. Department of Energy (DOE), Office of Basic Energy Sciences, Division of Chemical Sciences, Geosciences, and Biosciences, Catalysis Science Program, under Contract No. DE-AC-02-06CH11357. M.P.C. acknowledges the National Science Foundation (CHE-1800561) for support.

#### Notes

The authors declare no competing financial interest.

#### **■** REFERENCES

- (1) Koval, C. A.; Lercher, J.; Scott, S. L. Basic Research Needs for Catalysis Science to Transform Energy Technologies; U.S. Department of Energy, Office of Basic Energy SciencesGaithersburg, MD, 2017.
- (2) Munnik, P.; De Jongh, P. E.; De Jong, K. P. Recent Developments in the Synthesis of Supported Catalysts. *Chem. Rev.* **2015**, *115*, 6687–6718.
- (3) Schwarz, J. A.; Contescu, C.; Contescu, A. Methods for Preparation of Catalytic Materials. *Chem. Rev.* **1995**, 95, 477–510.
- (4) Eskandari, S.; Tate, G.; Leaphart, N. R.; Regalbuto, J. R. Nanoparticle Synthesis via Electrostatic Adsorption Using Incipient Wetness Impregnation. ACS Catal. 2018, 8, 10383–10391.
- (5) Serp, P.; Kalck, P.; Feurer, R. Chemical Vapor Deposition Methods for the Controlled Preparation of Supported Catalytic Materials. *Chem. Rev.* **2002**, *102*, 3085–3128.
- (6) Fujdala, K. L.; Tilley, T. D. Design and Synthesis of Heterogeneous Catalysts: The Thermolytic Molecular Precursor Approach. *J. Catal.* **2003**, *216*, 265–275.
- (7) Liu, L.; Corma, A. Metal Catalysts for Heterogeneous Catalysis: From Single Atoms to Nanoclusters and Nanoparticles. *Chem. Rev.* **2018**, *118*, 4981–5079.
- (8) Kondrat, S. A.; van Bokhoven, J. A. A Perspective on Counting Catalytic Active Sites and Rates of Reaction Using X-Ray Spectroscopy. *Top. Catal.* **2019**, *62*, 1218–1227.
- (9) Copéret, C.; Comas-Vives, A.; Conley, M. P.; Estes, D. P.; Fedorov, A.; Mougel, V.; Nagae, H.; Núnez-Zarur, F.; Zhizhko, P. A. Surface Organometallic and Coordination Chemistry toward Single-Site Heterogeneous Catalysts: Strategies, Methods, Structures, and Activities. Chem. Rev. 2016, 116, 323–421.
- (10) Samantaray, M. K.; D'Elia, V.; Pump, E.; Falivene, L.; Harb, M.; Ould Chikh, S.; Cavallo, L.; Basset, J. M. The Comparison between Single Atom Catalysis and Surface Organometallic Catalysis. *Chem. Rev.* 2020, 120, 734–813.
- (11) Conley, M. P.; Mougel, V.; Peryshkov, D. V.; Forrest, W. P.; Gajan, D.; Lesage, A.; Emsley, L.; Copéret, C.; Schrock, R. R. A Well-Defined Silica-Supported Tungsten Oxo Alkylidene Is a Highly Active Alkene Metathesis Catalyst. *J. Am. Chem. Soc.* **2013**, *135*, 19068–19070
- (12) Conley, M. P.; Forrest, W. P.; Mougel, V.; Copéret, C.; Schrock, R. R. Bulky Aryloxide Ligand Stabilizes a Heterogeneous Metathesis Catalyst. *Angew. Chem., Int. Ed.* **2014**, 53, 14221–14224.
- (13) van Leeuwen, P. W. N. M.; Chadwick, J. C. Homogeneous Catalysts: Activity Stability Deactivation; Wiley-VHC, 2011; pp 1–404.
- (14) Bailey, G. A.; Foscato, M.; Higman, C. S.; Day, C. S.; Jensen, V. R.; Fogg, D. E. Bimolecular Coupling as a Vector for Decomposition of Fast-Initiating Olefin Metathesis Catalysts. *J. Am. Chem. Soc.* **2018**, *140*, 6931–6944.
- (15) Kobayashi, T.; Perras, F. A.; Slowing, I. I.; Sadow, A. D.; Pruski, M. Dynamic Nuclear Polarization Solid-State NMR in Heterogeneous Catalysis Research. *ACS Catal.* **2015**, *5*, 7055–7062.
- (16) Lilly Thankamony, A. S.; Wittmann, J. J.; Kaushik, M.; Corzilius, B. Dynamic Nuclear Polarization for Sensitivity Enhancement in Modern Solid-State NMR. *Prog. Nucl. Magn. Reson. Spectrosc.* **2017**, *102–103*, 120–195.
- (17) Rossini, A. J.; Zagdoun, A.; Lelli, M.; Lesage, A.; Copéret, C.; Emsley, L. Dynamic Nuclear Polarization Surface Enhanced NMR Spectroscopy. *Acc. Chem. Res.* **2013**, *46*, 1942–1951.
- (18) Rossini, A. J. Materials Characterization by Dynamic Nuclear Polarization-Enhanced Solid-State NMR Spectroscopy. *J. Phys. Chem. Lett.* **2018**, *9*, 5150–5159.
- (19) De Groot, F. High-Resolution X-Ray Emission and X-Ray Absorption Spectroscopy. *Chem. Rev.* **2001**, *101*, 1779–1808.
- (20) Chen, L. X.; Zhang, X.; Shelby, M. L. Recent Advances on Ultrafast X-Ray Spectroscopy in the Chemical Sciences. *Chem. Sci.* **2014**, *5*, 4136–4152.
- (21) van Bokhoven, J. A.; Lamberti, C. State-of-the-Art X-Ray Spectroscopy in Catalysis. In Nanotechnology in Catalysis: Application

- in the Chemical Industry, Energy Development, and Environment Protection 2017, 1029-1054.
- (22) Bordiga, S.; Groppo, E.; Agostini, G.; Van Bokhoven, J. A.; Lamberti, C. Reactivity of Surface Species in Heterogeneous Catalysts Probed by in Situ X-Ray Absorption Techniques. *Chem. Rev.* **2013**, 113, 1736–1850.
- (23) Sautet, P.; Delbecq, F. Catalysis and Surface Organometallic Chemistry: A View from Theory and Simulations. *Chem. Rev.* **2010**, *110*, 1788–1806.
- (24) Pankin, I. A.; Martini, A.; Lomachenko, K. A.; Soldatov, A. V.; Bordiga, S.; Borfecchia, E. Identifying Cu-Oxo Species in Cu-Zeolites by XAS: A Theoretical Survey by DFT-Assisted XANES Simulation and EXAFS Wavelet Transform. *Catal. Today* **2020**, *345*, 125–135.
- (25) Gordon, C. P.; Shirase, S.; Yamamoto, K.; Andersen, R. A.; Eisenstein, O.; Copéret, C. NMR Chemical Shift Analysis Decodes Olefin Oligo- and Polymerization Activity of d<sup>0</sup> Group 4 Metal Complexes. *Proc. Natl. Acad. Sci. U. S. A.* **2018**, *115*, E5867–E5876.
- (26) Helgaker, T.; Jaszuński, M.; Ruud, K. Ab Initio Methods for the Calculation of NMR Shielding and Indirect Spin-Spin Coupling Constants. *Chem. Rev.* **1999**, *99*, 293–352.
- (27) Wegener, S. L.; Marks, T. J.; Stair, P. C. Design Strategies for the Molecular Level Synthesis of Supported Catalysts. *Acc. Chem. Res.* **2012**, *45*, 206–214.
- (28) Eisen, M. S.; Marks, T. J. Supported Organoactinide Complexes as Heterogeneous Catalysts. A Kinetic and Mechanistic Study of Facile Arene Hydrogenation. *J. Am. Chem. Soc.* **1992**, *114*, 10358–10368
- (29) Ahn, H.; Marks, T. J. Supported Organometallics. Highly Electrophilic Cationic Metallocene Hydrogenation and Polymerization Catalysts Formed via Protonolytic Chemisorption on Sulfated Zirconia. J. Am. Chem. Soc. 1998, 120, 13533–13534.
- (30) Dufaud, V.; Basset, J.-M. Catalytic Hydrogenolysis at Low Temperature and Pressure of Polyethylene and Polypropylene to Diesels or Lower Alkanes by a Zirconium Hydride Supported on Silica-Alumina: A Step Toward Polyolefin Degradation by the Microscopic Reverse of Ziegler-Natta Pol. Angew. Chem., Int. Ed. 1998, 37, 806–810.
- (31) Vidal, V.; Théolier, A.; Thivolle-Cazat, J.; Basset, J.-M.; Corker, J. Synthesis, Characterization, and Reactivity, in the C-H Bond Activation of Cycloalkanes, of a Silica-Supported Tantalum(III) Monohydride Complex: (:SiO)<sub>2</sub>Ta<sup>III</sup>-H. *J. Am. Chem. Soc.* **1996**, *118*, 4595–4602.
- (32) Vidal, V.; Theolier, A.; Thivolle-Cazat, J.; Basset, J. M. Metathesis of Alkanes Catalyzed by Silica-Supported Transition Metal Hydrides. *Science* **1997**, *276*, 99–102.
- (33) Rhers, B.; Salameh, A.; Baudouin, A.; Quadrelli, E. A.; Taoufik, M.; Copéret, C.; Lefebvre, F.; Basset, J.-M.; Solans-Monfort, X.; Eisenstein, O.; Lukens, W. W.; Lopez, L. P. H.; Sinha, A.; Schrock, R. R. A Well-Defined, Silica-Supported Tungsten Imido Alkylidene Olefin Metathesis Catalyst. *Organometallics* **2006**, *25*, 3554–3557.
- (34) Joubert, J.; Delbecq, F.; Sautet, P.; Le Roux, E.; Taoufik, M.; Thieuleux, C.; Blanc, F.; Copéret, C.; Thivolle-Cazat, J.; Basset, J.-M. Molecular Understanding of Alumina Supported Single-Site Catalysts by a Combination of Experiment and Theory. *J. Am. Chem. Soc.* **2006**, *128*, 9157–9169.
- (35) Blanc, F.; Thivolle-Cazat, J.; Basset, J.-M.; Copéret, C.; Hock, A. S.; Tonzetich, Z. J.; Schrock, R. R. Highly Active, Stable, and Selective Well-Defined Silica Supported Mo Imido Olefin Metathesis Catalysts. J. Am. Chem. Soc. 2007, 129, 1044–1045.
- (36) Alexeev, O. S.; Gates, B. C. Supported Bimetallic Cluster Catalysts. *Ind. Eng. Chem. Res.* **2003**, 42, 1571–1587.
- (37) Argo, A. M.; Odzak, J. F.; Lai, F. S.; Gates, B. C. Observation of Ligand Effects during Alkene Hydrogenation Catalysed by Supported Metal Clusters. *Nature* **2002**, *415*, 623–626.
- (38) Guzman, J.; Gates, B. C. Simultaneous Presence of Cationic and Reduced Gold in Functioning MgO-Supported CO Oxidation Catalysts: Evidence from X-Ray Absorption Spectroscopy. *J. Phys. Chem. B* **2002**, *106*, 7659–7665.

- (39) Nozaki, C.; Lugmair, C. G.; Bell, A. T.; Tilley, T. D. Synthesis, Characterization, and Catalytic Performance of Single-Site Iron(III) Centers on the Surface of SBA-15 Silica. *J. Am. Chem. Soc.* **2002**, *124*, 13194–13203.
- (40) Jarupatrakorn, J.; Tilley, T. D. Silica-Supported, Single-Site Titanium Catalysts for Olefin Epoxidation. A Molecular Precursor Strategy for Control of Catalyst Structure. J. Am. Chem. Soc. 2002, 124, 8380–8388.
- (41) Brutchey, R. L.; Ruddy, D. A.; Andersen, L. K.; Tilley, T. D. Influence of Surface Modification of Ti-SBA15 Catalysts on the Epoxidation Mechanism for Cyclohexene with Aqueous Hydrogen Peroxide. *Langmuir* **2005**, *21*, 9576–9583.
- (42) Ruddy, D. A.; Tilley, T. D. Kinetics and Mechanism of Olefin Epoxidation with Aqueous  $H_2O_2$  and a Highly Selective Surface-Modified TaSBA15 Heterogeneous Catalyst. *J. Am. Chem. Soc.* **2008**, 130, 11088–11096.
- (43) Amor Nait Ajjou, J.; Scott, S. L. Reactions of Tetraalkylchromium(IV) with Silica: Mechanism of Grafting and Characterization of Surface Organometallic Complexes. *Organometallics* 1997, 16, 86–92.
- (44) Amor Nait Ajjou, J.; Scott, S. L.; Paquet, V. Synthesis and Characterization of Silica-Stabilized Chromium(IV) Alkylidene Complexes. J. Am. Chem. Soc. 1998, 120, 415–416.
- (4S) Bouh, A. O.; Rice, G. L.; Scott, S. L. Mono- and Dinuclear Silica-Supported Titanium(IV) Complexes and the Effect of TiOTi Connectivity on Reactivity. *J. Am. Chem. Soc.* **1999**, *121*, 7201–7210.
- (46) Kaphan, D. M.; Klet, R. C.; Perras, F. A.; Pruski, M.; Yang, C.; Kropf, A. J.; Delferro, M. Surface Organometallic Chemistry of Supported Iridium(III) as a Probe for Organotransition Metal-Support Interactions in C-H Activation. *ACS Catal.* **2018**, *8*, 5363–5373.
- (47) Syed, Z. H.; Kaphan, D. M.; Perras, F. A.; Pruski, M.; Ferrandon, M. S.; Wegener, E. C.; Celik, G.; Wen, J.; Liu, C.; Dogan, F.; Goldberg, K. I.; Delferro, M. Electrophilic Organoiridium(III) Pincer Complexes on Sulfated Zirconia for Hydrocarbon Activation and Functionalization. J. Am. Chem. Soc. 2019, 141, 6325–6337.
- (48) Tafazolian, H.; Culver, D. B.; Conley, M. P. A Well-Defined Ni(II) α-Diimine Catalyst Supported on Sulfated Zirconia for Polymerization Catalysis. *Organometallics* **2017**, *36*, 2385–2388.
- (49) Li, Y.; Liu, J.; He, J.; Wang, L.; Lei, J. Silica/Titania Composite-Supported NiCo Catalysts with Combined Catalytic Effects for Phenol Hydrogenation under Fast and Mild Conditions. *Appl. Catal., A* **2020**, *591*, 117409.
- (50) Eedugurala, N.; Wang, Z.; Chaudhary, U.; Nelson, N.; Kandel, K.; Kobayashi, T.; Slowing, I. I.; Pruski, M.; Sadow, A. D. Mesoporous Silica-Supported Amidozirconium-Catalyzed Carbonyl Hydroboration. *ACS Catal.* **2015**, *5*, 7399–7414.
- (51) Le Roux, E.; Liang, Y.; Anwander, R. Silica-Grafted Neodymium Catalysts for the Production of Ultrahigh-Molecular-Weight Cis-1,4-Polyisoprene. *ChemCatChem* **2018**, *10*, 1905–1911.
- (52) Sonström, A.; Schneider, D.; Maichle-Mössmer, C.; Anwander, R. Titanium(IV) Catecholate-Grafted Mesoporous Silica KIT-6: Probing Sequential and Convergent Immobilization Approaches. *Eur. J. Inorg. Chem.* **2019**, 2019, 682–692.
- (53) Szeto, K. C.; Jones, Z. R.; Merle, N.; Rios, C.; Gallo, A.; Le Quemener, F.; Delevoye, L.; Gauvin, R. M.; Scott, S. L.; Taoufik, M. A Strong Support Effect in Selective Propane Dehydrogenation Catalyzed by  $Ga(i-Bu)_3$  Grafted onto  $\gamma$ -Alumina and Silica. *ACS Catal.* **2018**, *8*, 7566–7577.
- (54) Rouge, P.; Szeto, K. C.; Bouhoute, Y.; Merle, N.; De Mallmann, A.; Delevoye, L.; Gauvin, R. M.; Taoufik, M. Ethenolysis of Renewable Methyl Oleate Catalyzed by Readily Accessible Supported Group VI Oxo Catalysts. *Organometallics* **2020**, *39*, 1105–1111.
- (55) Zhuravlev, L. T. Concentration of Hydroxyl Groups on the Surface of Amorphous Silicas. *Langmuir* **1987**, *3*, 316–318.
- (56) Zhuravlev, L. T. The Surface Chemistry of Amorphous Silica. Zhuravlev Model. *Colloids Surf.*, A **2000**, 173, 1–38.
- (57) Lu, Y.; Cao, G.; Kale, R. P.; Prabakar, S.; Lopez, G. P.; Brinker, C. J. Microporous Silica Prepared by Organic Templating: Relation-

- ship between the Molecular Template and Pore Structure. *Chem. Mater.* 1999, 11, 1223–1229.
- (58) Trewyn, B. G.; Slowing, I. I.; Giri, S.; Chen, H. T.; Lin, V. S. Y. Synthesis and Functionalization of a Mesoporous Silica Nanoparticle Based on the Sol-Gel Process and Applications in Controlled Release. *Acc. Chem. Res.* **2007**, *40*, 846–853.
- (59) Zhao, D.; Feng, J.; Huo, Q.; Melosh, N.; Fredrickson, G. H.; Chmelka, B. F.; Stucky, G. D. Triblock Copolymer Syntheses of Mesoporous Silica with Periodic 50 to 300 Angstrom Pores. *Science* **1998**, 279, 548–552.
- (60) Lyaskovskyy, V.; De Bruin, B. Redox Non-Innocent Ligands: Versatile New Tools to Control Catalytic Reactions. *ACS Catal.* **2012**, 2, 270–279.
- (61) Luca, O. R.; Crabtree, R. H. Redox-Active Ligands in Catalysis. Chem. Soc. Rev. 2013, 42, 1440–1459.
- (62) van der Vlugt, J. I. Radical-Type Reactivity and Catalysis by Single-Electron Transfer to or from Redox-Active Ligands. *Chem. Eur. J.* **2019**, 25, 2651–2662.
- (63) Khan, F. F.; Chowdhury, A. D.; Lahiri, G. K. Bond Activations Assisted by Redox Active Ligand Scaffolds. *Eur. J. Inorg. Chem.* **2020**, 2020, 1138–1146.
- (64) Krossing, I.; Raabe, I. Noncoordinating Anions Fact or Fiction? A Survey of Likely Candidates. *Angew. Chem., Int. Ed.* **2004**, 43, 2066–2090.
- (65) Riddlestone, I. M.; Kraft, A.; Schaefer, J.; Krossing, I. Taming the Cationic Beast: Novel Developments in the Synthesis and Application of Weakly Coordinating Anions. *Angew. Chem., Int. Ed.* **2018**, *57*, 13982–14024.
- (66) Fisher, S. P.; Tomich, A. W.; Lovera, S. O.; Kleinsasser, J. F.; Guo, J.; Asay, M. J.; Nelson, H. M.; Lavallo, V. Nonclassical Applications of Closo-Carborane Anions: From Main Group Chemistry and Catalysis to Energy Storage. *Chem. Rev.* **2019**, *119*, 8262–8290.
- (67) Chen, E. Y. X.; Marks, T. J. Cocatalysts for Metal-Catalyzed Olefin Polymerization: Activators, Activation Processes, and Structure-Activity Relationships. *Chem. Rev.* **2000**, *100*, 1391–1434.
- (68) Stephan, D. W. Frustrated Lewis Pairs. J. Am. Chem. Soc. 2015, 137. 10018-10032.
- (69) Stephan, D. W.; Erker, G. Frustrated Lewis Pairs: Metal-Free Hydrogen Activation and More. *Angew. Chem., Int. Ed.* **2010**, 49, 46–
- (70) Stephan, D. W. Frustrated Lewis Pairs: From Concept to Catalysis. Acc. Chem. Res. 2015, 48, 306-316.
- (71) Fraenkel, D. Structure of Sulfated Metal Oxides and Its Correlation with Catalytic Activity. *Ind. Eng. Chem. Res.* **1997**, *36*, 52–59
- (72) Corma, A. Inorganic Solid Acids and Their Use in Acid-Catalyzed Hydrocarbon Reactions. *Chem. Rev.* 1995, 95, 559–614.
- (73) Hino, M.; Kobayashi, S.; Arata, K. Reactions of Butane and Isobutane Catalyzed by Zirconium Oxide Treated with Sulfate Ion. Solid Superacid Catalyst. *J. Am. Chem. Soc.* **1979**, *101*, 6439–6441.
- (74) Hino, M.; Arata, K. Synthesis of Solid Superacid Catalyst with Acid Strength of Ho. J. Chem. Soc., Chem. Commun. 1980, 851–852.
- (75) Haase, F.; Sauer, J. The Surface Structure of Sulfated Zirconia: Periodic Ab Initio Study of Sulfuric Acid Adsorbed on ZrO<sub>2</sub>(101) and ZrO<sub>2</sub>(001). *J. Am. Chem. Soc.* **1998**, *120*, 13503–13512.
- (76) Arata, K. Organic Syntheses Catalyzed by Superacidic Metal Oxides: Sulfated Zirconia and Related Compounds. *Green Chem.* **2009**, *11*, 1719–1728.
- (77) Li, X.; Nagaoka, K.; Simon, L. J.; Olindo, R.; Lercher, J. A.; Hofmann, A.; Sauer, J. Oxidative Activation of n-Butane on Sulfated Zirconia. *J. Am. Chem. Soc.* **2005**, *127*, 16159–16166.
- (78) Rodriguez, J.; Culver, D. B.; Conley, M. P. Generation of Phosphonium Sites on Sulfated Zirconium Oxide: Relationship to Brønsted Acid Strength of Surface -OH Sites. *J. Am. Chem. Soc.* **2019**, *141*. 1484–1488.
- (79) Fărcașiu, D.; Ghenciu, A.; Li, J. Q. The Mechanism of Conversion of Saturated Hydrocarbons Catalyzed by Sulfated Metal

- Oxides: Reaction of Adamantane on Sulfated Zirconia. *J. Catal.* **1996**, 158, 116–127.
- (80) Sarzanini, C.; Sacchero, G.; Pinna, F.; Signoretto, M.; Cerrato, G.; Morterra, C. Amount and Nature of Sulfates at the Surface of Sulfate-Doped Zirconia Catalysts. *J. Mater. Chem.* **1995**, *5*, 353–360.
- (81) Bochmann, M. The Chemistry of Catalyst Activation: The Case of Group 4 Polymerization Catalysts. *Organometallics* **2010**, 29, 4711–4740.
- (82) Delferro, M.; Marks, T. J. Multinuclear Olefin Polymerization Catalysts. *Chem. Rev.* **2011**, *111*, 2450–2485.
- (83) Nicholas, C. P.; Marks, T. J. Zirconium Hydrocarbyl Chemisorption on Sulfated Metal Oxides: New Supports, Chemisorption Pathways, and Implications for Catalysis. *Langmuir* **2004**, 20, 9456–9462.
- (84) Nicholas, C. P.; Marks, T. J. Sulfated Tin Oxide Nanoparticles as Supports for Molecule-Based Olefin Polymerization Catalysts. *Nano Lett.* **2004**, *4*, 1557–1559.
- (85) Stoyanov, E. S.; Kim, K. C.; Reed, C. A. An Infrared VNH Scale for Weakly Basic Anions. Implications for Single-Molecule Acidity and Superacidity. *J. Am. Chem. Soc.* **2006**, *128*, 8500–8508.
- (86) Klet, R. C.; Kaphan, D. M.; Liu, C.; Yang, C.; Kropf, A. J.; Perras, F. A.; Pruski, M.; Hock, A. S.; Delferro, M. Evidence for Redox Mechanisms in Organometallic Chemisorption and Reactivity on Sulfated Metal Oxides. J. Am. Chem. Soc. 2018, 140, 6308–6316.
- (87) Williams, L. A.; Guo, N.; Motta, A.; Delferro, M.; Fragalà, I. L.; Miller, J. T.; Marks, T. J. Surface Structural-Chemical Characterization of a Single-Site d<sup>0</sup> Heterogeneous Arene Hydrogenation Catalyst Having 100% Active Sites. *Proc. Natl. Acad. Sci. U. S. A.* **2013**, 110, 413–418.
- (88) Gu, W.; Stalzer, M. M.; Nicholas, C. P.; Bhattacharyya, A.; Motta, A.; Gallagher, J. R.; Zhang, G.; Miller, J. T.; Kobayashi, T.; Pruski, M.; Delferro, M.; Marks, T. J. Benzene Selectivity in Competitive Arene Hydrogenation: Effects of Single-Site Catalyst. acidic Oxide Surface Binding Geometry. J. Am. Chem. Soc. 2015, 137, 6770–6780.
- (89) Stalzer, M. M.; Nicholas, C. P.; Bhattacharyya, A.; Motta, A.; Delferro, M.; Marks, T. J. Single-Face/All-Cis Arene Hydrogenation by a Supported Single-Site d<sup>0</sup> Organozirconium Catalyst. *Angew. Chem., Int. Ed.* **2016**, 55, 5263–5267.
- (90) Williams, L. A.; Marks, T. J. Synthesis, Characterization, and Heterogeneous Catalytic Implementation of Sulfated Alumina Nanoparticles. Arene Hydrogenation and Olefin Polymerization Properties of Supported Organozirconium Complexes. *ACS Catal.* **2011**, *1*, 238–245.
- (91) Culver, D. B.; Tafazolian, H.; Conley, M. P. A Bulky Pd(II)  $\alpha$ -Diimine Catalyst Supported on Sulfated Zirconia for the Polymerization of Ethylene and Copolymerization of Ethylene and Methyl Acrylate. *Organometallics* **2018**, *37*, 1001–1006.
- (92) Johnson, L. K.; Mecking, S.; Brookhart, M. Copolymerization of Ethylene and Propylene with Functionalized Vinyl Monomers by Palladium(II) Catalysts. *J. Am. Chem. Soc.* **1996**, *118*, 267–268.
- (93) Klei, S. R.; Golden, J. T.; Burger, P.; Bergman, R. G. Cationic Ir(III) Alkyl and Hydride Complexes: Stoichiometric and Catalytic C-H Activation by Cp\*(PMe<sub>3</sub>)Ir(R)(X) in Homogeneous Solution. *J. Mol. Catal. A: Chem.* **2002**, *189*, 79–94.
- (94) Golden, J. T.; Andersen, R. A.; Bergman, R. G. Exceptionally Low-Temperature Carbon-Hydrogen/Carbon-Deuterium Exchange Reactions of Organic and Organometallic Compounds Catalyzed by the Cp\*(PMe<sub>3</sub>)IrH(ClCH<sub>2</sub>Cl)<sup>+</sup> Cation. J. Am. Chem. Soc. **2001**, 123, 5837–5838
- (95) Meyer, T. Y.; Woerpel, K. A.; Bergman, R. G.; Novak, B. M. Silica as a Ligand: Reactivity of the Iridium-Oxygen Bond of Cp\*Ir[Silica](Ph)(PMe<sub>3</sub>). *J. Am. Chem. Soc.* **1994**, *116*, 10290–10291
- (96) Gao, Y.; Guan, C.; Zhou, M.; Kumar, A.; Emge, T. J.; Wright, A. M.; Goldberg, K. I.; Krogh-Jespersen, K.; Goldman, A. S.  $\beta$ -Hydride Elimination and C-H Activation by an Iridium Acetate Complex, Catalyzed by Lewis Acids. Alkane Dehydrogenation Cocatalyzed by Lewis Acids and [2,6-Bis(4,4-Dimethyloxazolinyl)-

- 3,5-Dimethylphenyl]Iridium. J. Am. Chem. Soc. 2017, 139, 6338-6350
- (97) Benítez, V. M.; Yori, J. C.; Vera, C. R.; Pieck, C. L.; Grau, J. M.; Parera, J. M. Characterization of Transition-Metal Oxides Promoted with Oxoanions by Means of Test Reactions. *Ind. Eng. Chem. Res.* **2005**, *44*, 1716–1721.
- (98) Arata, K. In *Preparation of Superacidic Metal Oxides and Their Catalytic Action*; Jackson, S. D., Hargreaves, J. S. J., Eds.; Wiley-VHC Verlag GmbH & Co. KGaA: Weinheim, 2009; Vol. 2, pp 665–704.
- (99) Mougel, V.; Copéret, C. Magnitude and Consequence of OR Ligand σ-Donation on Alkene Metathesis Activity in D0 Silica Supported ( $\equiv$ SiO)W(NAr)( $\equiv$ CHtBu)(OR) Catalysts. *Chem. Sci.* **2014**, *5*, 2475–2481.
- (100) Conley, M. P.; Copéret, C.; Thieuleux, C. Mesostructured Hybrid Organic-Silica Materials: Ideal Supports for Well-Defined Heterogeneous Organometallic Catalysts. *ACS Catal.* **2014**, *4*, 1458–1469
- (101) Bendjeriou-Sedjerari, A.; Pelletier, J. D. A.; Abou-Hamad, E.; Emsley, L.; Basset, J. M. A Well-Defined Mesoporous Amine Silica Surface via a Selective Treatment of SBA-15 with Ammonia. *Chem. Commun.* **2012**, *48*, 3067–3069.
- (102) Bendjeriou-Sedjerari, A.; Azzi, J. M.; Abou-Hamad, E.; Anjum, D. H.; Pasha, F. A.; Huang, K. W.; Emsley, L.; Basset, J. M. Bipodal Surface Organometallic Complexes with Surface N-Donor Ligands and Application to the Catalytic Cleavage of C-H and C-C Bonds in n-Butane. *J. Am. Chem. Soc.* **2013**, *135*, 17943–17951.
- (103) Asefa, T.; Kruk, M.; Coombs, N.; Grondey, H.; MacLachlan, M. J.; Jaroniec, M.; Ozin, G. A. Novel Route to Periodic Mesoporous Aminosilicas, PMAs: Ammonolysis of Periodic Mesoporous Organosilicas. *J. Am. Chem. Soc.* **2003**, *125*, 11662–11673.
- (104) Pasha, F. A.; Bendjeriou-Sedjerari, A.; Huang, K. W.; Basset, J. M. C-H and C-C Activation of n -Butane with Zirconium Hydrides Supported on SBA15 Containing N-Donor Ligands:  $[(\equiv SiNH-)(\equiv SiX-)ZrH_2]$ ,  $[(\equiv SiNH-)(\equiv SiX-)ZzrH]$ , and  $[(\equiv SiN=)(\equiv SiX-)ZrH]$  (X = -NH-, -O-). A DFT Study. Organometallics 2014, 33, 3320–3327.
- (105) Bendjeriou-Sedjerari, A.; Sofack-Kreutzer, J.; Minenkov, Y.; Abou-Hamad, E.; Hamzaoui, B.; Werghi, B.; Anjum, D. H.; Cavallo, L.; Huang, K. W.; Basset, J. M. Tungsten(VI) Carbyne/Bis(Carbene) Tautomerization Enabled by N-Donor SBA15 Surface Ligands: A Solid-State NMR and DFT Study. *Angew. Chem., Int. Ed.* **2016**, 55, 11162–11166.
- (106) Le Roux, E.; Taoufik, M.; Chabanas, M.; Alcor, D.; Baudouin, A.; Copéret, C.; Thivolle-Cazat, J.; Basset, J. M.; Lesage, A.; Hediger, S.; Emsley, L. Well-Defined Surface Tungstenocarbyne Complexes through the Reaction of  $[W(\equiv CtBu)(CH_2tBu)_3]$  with Silica. Organometallics 2005, 24, 4274–4279.
- (107) Le Roux, E.; Taoufik, M.; Copéret, C.; De Mallmann, A.; Thivolle-Cazat, J.; Basset, J. M.; Maunders, B. M.; Sunley, G. J. Development of Tungsten-Based Heterogeneous Alkane Metathesis Catalysts through a Structure-Activity Relationship. *Angew. Chem., Int. Ed.* **2005**, *44*, 6755–6758.
- (108) Adams, G. M.; Weller, A. S. POP-Type Ligands: Variable Coordination and Hemilabile Behaviour. *Coord. Chem. Rev.* **2018**, 355, 150–172.
- (109) Xu, T.; Kob, N.; Drago, R. S.; Nicholas, J. B.; Haw, J. F. A Solid Acid Catalyst at the Threshold of Superacid Strength: NMR, Calorimetry, and Density Functional Theory Studies of Silica-Supported Aluminum Chloride. *J. Am. Chem. Soc.* **1997**, *119*, 12231–12239.
- (110) Olah, G. A.; Prakash, G. K. S.; Sommer, J.; Molnar, A. Superacid Chemistry; John Wiley & Sons, Ltd, 2009, 1.
- (111) Yamamoto, H.; Futatsugi, K. Designer Acids": Combined Acid Catalysis for Asymmetric Synthesis. *Angew. Chem., Int. Ed.* **2005**, 44, 1924–1942.
- (112) Walzer, J. F. Supported Ionic Catalyst Composition. U.S. Patent 5643847, 1995.
- (113) Millot, N.; Santini, C. C.; Baudouin, A.; Basset, J. M. Supported Cationic Complexes: Selective Preparation and Character-

- ization of the Well-Defined Electrophilic Metallocenium Cation  $[\equiv SiO-B(C_6F_5)_3]^-[Cp*ZrMe_2(Et_2NPh)]^+$  Supported on Silica. *Chem. Commun.* **2003**, 3, 2034–2035.
- (114) Wanglee, Y. J.; Hu, J.; White, R. E.; Lee, M. Y.; Stewart, S. M.; Perrotin, P.; Scott, S. L. Borane-Induced Dehydration of Silica and the Ensuing Water-Catalyzed Grafting of  $B(C_6F_5)_3$  to Give a Supported, Single-Site Lewis Acid,  $\equiv SiOB(C_6F_5)_2$ . J. Am. Chem. Soc. 2012, 134, 355–366.
- (115) Müller, L. O.; Himmel, D.; Stauffer, J.; Steinfeld, G.; Slattery, J.; Santiso-Quiñones, G.; Brecht, V.; Krossing, I. Simple Access to the Non-Oxidizing Lewis Superacid PhF→Al(ORF)<sub>3</sub> (RF = C (CF<sub>3</sub>)3). *Angew. Chem., Int. Ed.* **2008**, 47, 7659–7663.
- (116) Culver, D. B.; Venkatesh, A.; Huynh, W.; Rossini, A. J.; Conley, M. P. Al(ORF)3 (RF =  $C(CF_3)_3$ ) Activated Silica: A Well-Defined Weakly Coordinating Surface Anion. *Chem. Sci.* **2020**, *11*, 1510–1517.
- (117) Camacho-Bunquin, J.; Ferrandon, M.; Sohn, H.; Yang, D.; Liu, C.; Ignacio-De Leon, P. A.; Perras, F. A.; Pruski, M.; Stair, P. C.; Delferro, M. Chemoselective Hydrogenation with Supported Organoplatinum(IV) Catalyst on Zn(II)-Modified Silica. *J. Am. Chem. Soc.* 2018, 140, 3940–3951.
- (118) Qi, Z.; Xiao, C.; Liu, C.; Goh, T. W.; Zhou, L.; Maligal-Ganesh, R.; Pei, Y.; Li, X.; Curtiss, L. A.; Huang, W. Sub-4 Nm PtZn Intermetallic Nanoparticles for Enhanced Mass and Specific Activities in Catalytic Electrooxidation Reaction. *J. Am. Chem. Soc.* **2017**, *139*, 4762–4768.
- (119) Cybulskis, V. J.; Bukowski, B. C.; Tseng, H. T.; Gallagher, J. R.; Wu, Z.; Wegener, E.; Kropf, A. J.; Ravel, B.; Ribeiro, F. H.; Greeley, J.; Miller, J. T. Zinc Promotion of Platinum for Catalytic Light Alkane Dehydrogenation: Insights into Geometric and Electronic Effects. ACS Catal. 2017, 7, 4173–4181.
- (120) Iihama, S.; Furukawa, S.; Komatsu, T. Efficient Catalytic System for Chemoselective Hydrogenation of Halonitrobenzene to Haloniline Using PtZn Intermetallic Compound. *ACS Catal.* **2016**, *6*, 742–746.
- (121) Liberman-Martin, A. L.; Bergman, R. G.; Tilley, T. D. A Remote Lewis Acid Trigger Dramatically Accelerates Biaryl Reductive Elimination from a Platinum Complex. *J. Am. Chem. Soc.* **2013**, *135*, 9612–9615.
- (122) Liberman-Martin, A. L.; Ziegler, M. S.; DiPasquale, A. G.; Bergman, R. G.; Tilley, T. D. Functionalization of an Iridium-Diamidocarbene Complex by Ligand-Based Reactions with Titanocene and Zirconocene Sources. *Polyhedron* **2016**, *116*, 111–115.
- (123) Liberman-Martin, A. L.; Levine, D. S.; Ziegler, M. S.; Bergman, R. G.; Tilley, T. D. Lewis Acid-Base Interactions between Platinum(II) Diaryl Complexes and Bis(Perfluorophenyl)Zinc: Strongly Accelerated Reductive Elimination Induced by a Z-Type Ligand. Chem. Commun. 2016, 52, 7039–7042.
- (124) Liberman-Martin, A. L.; Levine, D. S.; Liu, W.; Bergman, R. G.; Tilley, T. D. Biaryl Reductive Elimination Is Dramatically Accelerated by Remote Lewis Acid Binding to a 2,2'-Bipyrimidyl-Platinum Complex: Evidence for a Bidentate Ligand Dissociation Mechanism. *Organometallics* **2016**, *35*, 1064–1069.
- (125) Owen, J. S.; Labinger, J. A.; Bercaw, J. E. Kinetics and Mechanism of Methane, Methanol, and Dimethyl Ether C-H Activation with Electrophilic Platinum Complexes. *J. Am. Chem. Soc.* **2006**, *128*, 2005–2016.
- (126) Labinger, J. A. Platinum-Catalyzed C-H Functionalization. *Chem. Rev.* **2017**, *117*, 8483–8496.
- (127) Farneth, W. E.; Gorte, R. J. Methods for Characterizing Zeolite Acidity. *Chem. Rev.* 1995, 95, 615–635.
- (128) Boronat, M.; Corma, A. What Is Measured When Measuring Acidity in Zeolites with Probe Molecules? *ACS Catal.* **2019**, *9*, 1539–1548.
- (129) Chen, W.; Yi, X.; Huang, L.; Liu, W.; Li, G.; Acharya, D.; Sun, X.; Zheng, A. Can Hammett Indicators Accurately Measure the Acidity of Zeolite Catalysts with Confined Space? Insights into the Mechanism of Coloration. *Catal. Sci. Technol.* **2019**, *9*, 5045–5057.

- (130) Drago, R. S.; Kob, N. Acidity and Reactivity of Sulfated Zirconia and Metal-Doped Sulfated Zirconia. *J. Phys. Chem. B* **1997**, *101*, 3360–3364.
- (131) Haw, J. F.; Zhang, J.; Shimizu, K.; Venkatraman, T. N.; Luigi, D. P.; Song, W.; Barich, D. H.; Nicholas, J. B. NMR and Theoretical Study of Acidity Probes on Sulfated Zirconia Catalysts. *J. Am. Chem. Soc.* **2000**, *122*, 12561–12570.
- (132) Gansmüller, A.; Simorre, J. P.; Hediger, S. Windowed R-PDLF Recoupling: A Flexible and Reliable Tool to Characterize Molecular Dynamics. *J. Magn. Reson.* **2013**, 234, 154–164.
- (133) Larsen, F. H.; Jakobsen, H. J.; Ellis, P. D.; Nielsen, N. C. QCPMG-MAS NMR of Half-Integer Quadrupolar Nuclei. *J. Magn. Reson.* 1998, 131, 144–147.
- (134) Perras, F. A.; Wang, Z.; Naik, P.; Slowing, I. I.; Pruski, M. Natural Abundance <sup>17</sup>O DNP NMR Provides Precise O-H Distances and Insights into the Brønsted Acidity of Heterogeneous Catalysts. *Angew. Chem., Int. Ed.* **2017**, *56*, 9165–9169.
- (135) Zheng, A.; Liu, S.-B.; Deng, F. 31P NMR Chemical Shifts of Phosphorus Probes as Reliable and Practical Acidity Scales for Solid and Liquid Catalysts. *Chem. Rev.* 2017, 117, 12475–12531.
- (136) Reed, C. A. The Silylium Ion Problem, R<sub>3</sub>Si<sup>+</sup>. Bridging Organic and Inorganic Chemistry. *Acc. Chem. Res.* **1998**, *31*, 325–332.
- (137) Culver, D. B.; Conley, M. P. Activation of C-F Bonds by Electrophilic Organosilicon Sites Supported on Sulfated Zirconia. *Angew. Chem., Int. Ed.* **2018**, *57*, 14902–14905.
- (138) Song, W.; Marcus, D. M.; Abubakar, S. M.; Jani, E.; Haw, J. F. Trimethylsilylation of Framework Brønsted Acid Sites in Microporous Zeolites and Silico-Aluminophosphates. *J. Am. Chem. Soc.* **2003**, *125*, 13964–13965.
- (139) Zapilko, C.; Widenmeyer, M.; Nagl, I.; Estler, F.; Anwander, R.; Raudaschl-Sieber, G.; Groeger, O.; Engelhardt, G. Advanced Surface Functionalization of Periodic Mesoporous Silica: Kinetic Control by Trisilazane Reagents. *J. Am. Chem. Soc.* **2006**, *128*, 16266–16276.
- (140) Behringer, K. D.; Blümel, J. Reactions of Ethoxysilanes with Silica: A Solid-State NMR Study. *J. Liq. Chromatogr. Relat. Technol.* **1996**, *19*, 2753–2765.
- (141) Blümel, J. Reactions of Ethoxysilanes with Silica: A Solid-State NMR Study. J. Am. Chem. Soc. 1995, 117, 2112–2113.
- (142) Huynh, W.; Conley, M. P. Origin of the  $^{29}$ Si NMR Chemical Shift in  $R_3$ Si-X and Relationship to the Formation of Silylium ( $R_3$ Si+) Ions. *Dalton Trans.* **2020**. DOI: 10.1039/D0DT02099K
- (143) Kašpar, J.; Fornasiero, P.; Hickey, N. Automotive Catalytic Converters: Current Status and Some Perspectives. *Catal. Today* **2003**, *77*, 419–449.
- (144) Granger, P.; Parvulescu, V. I. Catalytic  $NO_x$  Abatement Systems for Mobile Sources: From Three-Way to Lean Burn after-Treatment Technologies. *Chem. Rev.* **2011**, *111*, 3155–3207.
- (145) Diwell, A. F.; Rajaram, R. R.; Shaw, H. A.; Truex, T. J. The Role of Ceria in Three-Way Catalysts. In *Studies in Surface Science and Catalysis*; Crucq, A., Ed.; Elsevier, 1991; Vol. 71, pp 139–152.
- (146) van Deelen, T. W.; Hernández Mejía, C.; de Jong, K. P. Control of Metal-Support Interactions in Heterogeneous Catalysts to Enhance Activity and Selectivity. *Nat. Catal.* **2019**, *2*, 955–970.
- (147) Yang, Y.; Mims, C. A.; Mei, D. H.; Peden, C. H. F.; Campbell, C. T. Mechanistic Studies of Methanol Synthesis over Cu from CO/CO<sub>2</sub>/H<sub>2</sub>/H<sub>2</sub>O Mixtures: The Source of C in Methanol and the Role of Water. *J. Catal.* **2013**, 298, 10–17.
- (148) Bruix, A.; Rodriguez, J. A.; Ramírez, P. J.; Senanayake, S. D.; Evans, J.; Park, J. B.; Stacchiola, D.; Liu, P.; Hrbek, J.; Illas, F. A New Type of Strong Metal-Support Interaction and the Production of  $\rm H_2$  through the Transformation of Water on  $\rm Pt/CeO_2(111)$  and  $\rm Pt/CeO_x/TiO_2(110)$  Catalysts. *J. Am. Chem. Soc.* **2012**, *134*, 8968–8974. (149) Gunasooriya, G. T. K. K.; Seebauer, E. G.; Saeys, M. Ethylene Hydrogenation over  $\rm Pt/TiO_2$ : A Charge-Sensitive Reaction. *ACS*
- (150) Ioannides, T.; Verykios, X. E. Charge Transfer in Metal Catalysts Supported on Doped TiO<sub>2</sub>: A Theoretical Approach Based

Catal. 2017, 7, 1966-1970.

- on Metal-Semiconductor Contact Theory. J. Catal. 1996, 161, 560–569.
- (151) Schwab, G. M.; Koller, K. Combined Action of Metal and Semiconductor Catalysts. J. Am. Chem. Soc. 1968, 90, 3078–3080.
- (152) Iwasawa, Y.; Sato, H. Preparations of  ${\rm TiO_2}$ -Attached Rh Catalysts and Their Catalysis. *Chem. Lett.* **1985**, *14*, 507–510.
- (153) Jeantelot, G.; Qureshi, M.; Harb, M.; Ould-Chikh, S.; Anjum, D. H.; Abou-Hamad, E.; Aguilar-Tapia, A.; Hazemann, J.-L.; Takanabe, K.; Basset, J.-M. TiO<sub>2</sub>-Supported Pt Single Atoms by Surface Organometallic Chemistry for Photocatalytic Hydrogen Evolution. *Phys. Chem. Chem. Phys.* **2019**, *21*, 24429–24440.
- (154) Grasser, S.; Haeßner, C.; Köhler, K.; Lefebvre, F.; Basset, J. M. Structures of Paramagnetic VIV Amido Complexes Grafted onto Metal Oxide Surfaces: Model Systems for Heterogeneous Vanadium Catalysts. *Phys. Chem. Chem. Phys.* **2003**, *5*, 1906–1911.
- (155) Dufour, P.; Houtman, C.; Santini, C. C.; Nedez, C.; Basset, J. M.; Hsu, L. Y.; Shore, S. G. Surface Organometallic Chemistry: Reaction of Tris(Allyl)Rhodium with Surfaces of Silica, Alumina, Titania and Magnesia. *J. Am. Chem. Soc.* **1992**, *114*, 4248–4257.
- (156) Aguilar-Guerrero, V.; Gates, B. C. Genesis of a Highly Active Cerium Oxide-Supported Gold Catalyst for CO Oxidation. *Chem. Commun.* **2007**, *30*, 3210–3212.
- (157) Guzman, J.; Kuba, S.; Fierro-Gonzalez, J. C.; Gates, B. C. Formation of Gold Clusters on TiO<sub>2</sub> from Adsorbed Au(CH 3)2(C5H7O2): Characterization by X-Ray Absorption Spectroscopy. *Catal. Lett.* **2004**, *95*, 77–86.
- (158) Sheehan, S. W.; Thomsen, J. M.; Hintermair, U.; Crabtree, R. H.; Brudvig, G. W.; Schmuttenmaer, C. A. A Molecular Catalyst for Water Oxidation That Binds to Metal Oxide Surfaces. *Nat. Commun.* **2015**. *6*. 1–9.
- (159) Lebedev, D.; Ezhov, R.; Heras-Domingo, J.; Comas-Vives, A.; Kaeffer, N.; Willinger, M.; Solans-Monfort, X.; Huang, X.; Pushkar, Y.; Copéret, C. Atomically Dispersed Iridium on Indium Tin Oxide Efficiently Catalyzes Water Oxidation. ACS Cent. Sci. 2020, 6, 1189–1198
- (160) Fan, L.; Long, J.; Gu, Q.; Huang, H.; Lin, H.; Wang, X. Single-Site Nickel-Grafted Anatase TiO<sub>2</sub> for Hydrogen Production: Toward Understanding the Nature of Visible-Light Photocatalysis. *J. Catal.* **2014**, 320, 147–159.
- (161) Huang, H.; Lin, J.; Zhu, G.; Weng, Y.; Wang, X.; Fu, X.; Long, J. A Long-Lived Mononuclear Cyclopentadienyl Ruthenium Complex Grafted onto Anatase TiO<sub>2</sub> for Efficient CO<sub>2</sub> Photoreduction. *Angew. Chem., Int. Ed.* **2016**, *55*, 8314–8318.
- (162) Yamada, Y.; Kanemitsu, Y. Determination of Electron and Hole Lifetimes of Rutile and Anatase TiO<sub>2</sub> Single Crystals. *Appl. Phys. Lett.* **2012**, *101*, 133907.
- (163) Dzwigaj, S.; Arrouvel, C.; Breysse, M.; Geantet, C.; Inoue, S.; Toulhoat, H.; Raybaud, P. DFT Makes the Morphologies of Anatase-TiO<sub>2</sub> Nanoparticles Visible to IR Spectroscopy. *J. Catal.* **2005**, 236, 245–250.
- (164) Li, Y.-F.; Liu, Z.-P.; Liu, L.; Gao, W. Mechanism and Activity of Photocatalytic Oxygen Evolution on Titania Anatase in Aqueous Surroundings. *J. Am. Chem. Soc.* **2010**, *132*, 13008–13015.
- (165) Fröschl, T.; Hörmann, U.; Kubiak, P.; Kučerová, G.; Pfanzelt, M.; Weiss, C. K.; Behm, R. J.; Hüsing, N.; Kaiser, U.; Landfester, K.; Wohlfahrt-Mehrens, M. High Surface Area Crystalline Titanium Dioxide: Potential and Limits in Electrochemical Energy Storage and Catalysis. Chem. Soc. Rev. 2012, 41, 5313–5360.
- (166) Jeantelot, G.; Ould-Chikh, S.; Sofack-Kreutzer, J.; Abou-Hamad, E.; Anjum, D. H.; Lopatin, S.; Harb, M.; Cavallo, L.; Basset, J.-M. Morphology Control of Anatase TiO<sub>2</sub> for Well-Defined Surface Chemistry. *Phys. Chem. Chem. Phys.* **2018**, 20, 14362–14373.
- (167) Chapovetsky, A.; Langeslay, R. R.; Celik, G.; Perras, F. A.; Pruski, M.; Ferrandon, M. S.; Wegener, E. C.; Kim, H.; Dogan, F.; Wen, J.; Khetrapal, N.; Sharma, P.; White, J.; Kropf, A. J.; Sattelberger, A. P.; Kaphan, D. M.; Delferro, M. Activation of Low-Valent, Multiply M-M Bonded Group VI Dimers toward Catalytic Olefin Metathesis via Surface Organometallic Chemistry. *Organometallics* **2020**, 39, 1035–1045.

- (168) Gonçalves, J. E.; Castro, S. C.; Ramos, A. Y.; Alves, M. C. M.; Gushikem, Y. X-Ray Absorption and XPS Study of Titanium Mixed Oxides Synthesized by the Sol-Gel Method. *J. Electron Spectrosc. Relat. Phenom.* **2001**, *114–116*, 307–311.
- (169) Boehm, H.-P.; Knözinger, H. In Nature and Estimation of Functional Groups on Solid Surfaces BT Catalysis: Science and Technology; Anderson, J. R., Boudart, M., Eds.; Springer Berlin Heidelberg: Berlin, Heidelberg, 1983; pp 39–207.
- (170) Martens, J. H. A.; Prins, R.; Zandbergen, H.; Koningsberger, D. C. Structure of Rhodium/Titania in the Normal and the SMSI State as Determined by Extended X-Ray Absorption Fine Structure and High-Resolution Transmission Electron Microscopy. *J. Phys. Chem.* 1988, 92, 1903–1916.
- (171) Luca, O. R.; Crabtree, R. H. Redox-Active Ligands in Catalysis. Chem. Soc. Rev. 2013, 42, 1440–1459.
- (172) Singh, B.; Indra, A. Role of Redox Active and Redox Non-Innocent Ligands in Water Splitting. *Inorg. Chim. Acta* **2020**, 506, 119440.
- (173) Mondal, B.; Ye, S. Hidden Ligand Noninnocence: A Combined Spectroscopic and Computational Perspective. *Coord. Chem. Rev.* **2020**, *405*, 213115.
- (174) Hojilla Atienza, C. C.; Milsmann, C.; Semproni, S. P.; Turner, Z. R.; Chirik, P. J. Reversible Carbon-Carbon Bond Formation Induced by Oxidation and Reduction at a Redox-Active Cobalt Complex. *Inorg. Chem.* **2013**, *52*, 5403–5417.
- (175) Darmon, J. M.; Stieber, S. C. E.; Sylvester, K. T.; Fernández, I.; Lobkovsky, E.; Semproni, S. P.; Bill, E.; Wieghardt, K.; Debeer, S.; Chirik, P. J. Oxidative Addition of Carbon-Carbon Bonds with a Redox-Active Bis(Imino)Pyridine Iron Complex. J. Am. Chem. Soc. 2012. 134, 17125—17137.
- (176) Tondreau, A. M.; Milsmann, C.; Patrick, A. D.; Hoyt, H. M.; Lobkovsky, E.; Wieghardt, K.; Chirik, P. J. Synthesis and Electronic Structure of Cationic, Neutral, and Anionic Bis(Imino)Pyridine Iron Alkyl Complexes: Evaluation of Redox Activity in Single-Component Ethylene Polymerization Catalysts. *J. Am. Chem. Soc.* **2010**, *132*, 15046–15059.
- (177) Bouwkamp, M. W.; Bowman, A. C.; Lobkovsky, E.; Chirik, P. J. Iron-Catalyzed  $[2\pi + 2\pi]$  Cycloaddition of  $\alpha,\omega$ -Dienes: The Importance of Redox-Active Supporting Ligands. *J. Am. Chem. Soc.* **2006**, *128*, 13340–13341.
- (178) Nie, J.; Patrocinio, A. O. T.; Hamid, S.; Sieland, F.; Sann, J.; Xia, S.; Bahnemann, D. W.; Schneider, J. New Insights into the Plasmonic Enhancement for Photocatalytic H<sub>2</sub> Production by Cu-TiO<sub>2</sub> upon Visible Light Illumination. *Phys. Chem. Chem. Phys.* **2018**, 20, 5264–5273.
- (179) Chiarello, G. L.; Ferri, D.; Selli, E. Effect of the CH<sub>3</sub>OH/H<sub>2</sub>O Ratio on the Mechanism of the Gas-Phase Photocatalytic Reforming of Methanol on Noble Metal-Modified TiO<sub>2</sub>. *J. Catal.* **2011**, 280, 168–177
- (180) Topsoe, N. Y.; Topsoe, H.; Dumesic, J. A. Vanadia/Titania Catalysts for Selective Catalytic Reduction (SCR) of Nitric-Oxide by Ammonia: I. Combined Temperature-Programmed in-Situ FTIR and On-Line Mass-Spectroscopy Studies. *J. Catal.* **1995**, *151*, 226–240.
- (181) Dhakshinamoorthy, A.; Navalon, S.; Corma, A.; Garcia, H. Photocatalytic CO<sub>2</sub> Reduction by TiO<sub>2</sub> and Related Titanium Containing Solids. *Energy Environ. Sci.* **2012**, *5*, 9217–9233.
- (182) Zhai, L.; Cui, C.; Zhao, Y.; Zhu, X.; Han, J.; Wang, H.; Ge, Q. Titania-Modified Silver Electrocatalyst for Selective CO<sub>2</sub> Reduction to CH<sub>3</sub>OH and CH<sub>4</sub> from DFT Study. *J. Phys. Chem. C* **2017**, *121*, 16275–16282.
- (183) Domestici, C.; Tensi, L.; Zaccaria, F.; Kissimina, N.; Valentini, M.; D'Amato, R.; Costantino, F.; Zuccaccia, C.; Macchioni, A. Molecular and Heterogenized Dinuclear Ir-Cp\* Water Oxidation Catalysts Bearing EDTA or EDTMP as Bridging and Anchoring Ligands. Sci. Bull. 2020, 65, 1614–1625.
- (184) Shin, H. H.; McIntosh, S. Proton-Conducting Perovskites as Supports for Cr Catalysts in Short Contact Time Ethane Dehydrogenation. *ACS Catal.* **2015**, *5*, 95–103.

- (185) Choi, S.; Choi, S. M.; Yoon, K. J.; Son, J.-W.; Lee, J.-H.; Kim, B.-K.; Sang, B.-I.; Kim, H. Collateral Hydrogenation over Proton-Conducting Ni/BaZr $_{0.85}$ Y $_{0.15}$ O $_{3-\delta}$  Catalysts for Promoting CO $_2$  Methanation. *RSC Adv.* **2018**, *8*, 32095–32101.
- (186) Humphreys, J.; Lan, R.; Du, D.; Xu, W.; Tao, S. Promotion Effect of Proton-Conducting Oxide  $BaZr_{0.1}Ce_{0.7}Y_{0.2}O_{3-\delta}$  on the Catalytic Activity of Ni towards Ammonia Synthesis from Hydrogen and Nitrogen. *Int. J. Hydrogen Energy* **2018**, 43, 17726–17736.
- (187) Mohamed, M. M.; Salama, T. M.; Yamaguchi, T. Synthesis, Characterization and Catalytic Properties of Titania-Silica Catalysts. *Colloids Surf., A* **2002**, 207, 25–32.
- (188) López, R.; Gómez, R.; Llanos, M. E. Photophysical and Photocatalytic Properties of Nanosized Copper-Doped Titania Sol-Gel Catalysts. *Catal. Today* **2009**, *148*, 103–108.
- (189) Andreeva, D.; Ivanov, I.; Ilieva, L.; Abrashev, M. V.; Zanella, R.; Sobczak, J. W.; Lisowski, W.; Kantcheva, M.; Avdeev, G.; Petrov, K. Gold Catalysts Supported on Ceria Doped by Rare Earth Metals for Water Gas Shift Reaction: Influence of the Preparation Method. *Appl. Catal., A* **2009**, 357, 159–169.
- (190) Sharma, S.; Hu, Z.; Zhang, P.; McFarland, E. W.; Metiu, H. CO<sub>2</sub> Methanation on Ru-Doped Ceria. *J. Catal.* **2011**, 278, 297–309.
- (191) Tabakova, T.; Ilieva, L.; Ivanov, I.; Zanella, R.; Sobczak, J. W.; Lisowski, W.; Kaszkur, Z.; Andreeva, D. Influence of the Preparation Method and Dopants Nature on the WGS Activity of Gold Catalysts Supported on Doped by Transition Metals Ceria. *Appl. Catal., B* **2013**, 136–137, 70–80.
- (192) López, J. M.; Gilbank, A. L.; García, T.; Solsona, B.; Agouram, S.; Torrente-Murciano, L. The Prevalence of Surface Oxygen Vacancies over the Mobility of Bulk Oxygen in Nanostructured Ceria for the Total Toluene Oxidation. *Appl. Catal., B* **2015**, *174*–175, 403–412.
- (193) Campbell, C. T.; Peden, C. H. F. Oxygen Vacancies and Catalysis on Ceria Surfaces. *Science* **2005**, *309*, 713–714.
- (194) Zou, X.; Liu, J.; Su, J.; Zuo, F.; Chen, J.; Feng, P. Facile Synthesis of Thermal- and Photostable Titania with Paramagnetic Oxygen Vacancies for Visible-Light Photocatalysis. *Chem. Eur. J.* **2013**, *19*, 2866–2873.
- (195) Lira, E.; Wendt, S.; Huo, P.; Hansen, J. Ø.; Streber, R.; Porsgaard, S.; Wei, Y.; Bechstein, R.; Lægsgaard, E.; Besenbacher, F. The Importance of Bulk Ti<sup>3+</sup> Defects in the Oxygen Chemistry on Titania Surfaces. *J. Am. Chem. Soc.* **2011**, *133*, 6529–6532.
- (196) Schwab, G. M.; Gossner, K. Heterogeneous Catalysis. Annu. Rev. Phys. Chem. 1963, 14, 177–204.
- (197) Schubert, B.; Gocke, E.; Schöllhorn, R.; Alonso-Vante, N.; Tributsch, H. In Situ X-Ray-Electrochemical Studies on the Origin of  $\rm H_2O_2$  Production during Oxygen Reduction at Transition Metal Cluster Materials. *Electrochim. Acta* **1996**, *41*, 1471–1478.
- (198) Vante, N. A.; Tributsch, H. Energy Conversion Catalysis Using Semiconducting Transition Metal Cluster Compounds. *Nature* **1986**, 323, 431–432.
- (199) Alexeev, O.; Gates, B. C. EXAFS Characterization of Supported Metal-Complex and Metal-Cluster Catalysts Made from Organometallic Precursors. *Top. Catal.* **2000**, *10*, 273–293.
- (200) Kephart, J. A.; Mitchell, B. S.; Chirila, A.; Anderton, K. J.; Rogers, D.; Kaminsky, W.; Velian, A. Atomically Defined Nanopropeller Fe<sub>3</sub>Co<sub>6</sub>Se<sub>8</sub>(Ph<sub>2</sub>PNTol)<sub>6</sub>: Functional Model for the Electronic Metal-Support Interaction Effect and High Catalytic Activity for Carbodiimide Formation. *J. Am. Chem. Soc.* **2019**, *141*, 19605–19610.
- (201) Hernández Sánchez, R.; Champsaur, A. M.; Choi, B.; Wang, S. G.; Bu, W.; Roy, X.; Chen, Y.-S.; Steigerwald, M. L.; Nuckolls, C.; Paley, D. W. Electron Cartography in Clusters. *Angew. Chem., Int. Ed.* **2018**, *57*, 13815–13820.
- (202) Hernández Sánchez, R.; Zheng, S.-L.; Betley, T. A. Ligand Field Strength Mediates Electron Delocalization in Octahedral [(HL)<sub>2</sub>Fe<sub>6</sub>(L')<sub>m</sub>]<sup>n+</sup> Clusters. *J. Am. Chem. Soc.* **2015**, *137*, 11126–11143.
- (203) Kashiwa, N.; Fujimura, H.; Tokuzumi, Y.  $MgCl_2$  Supports ZN Cats. Japanese Patent 1031698, 1968.

- (204) Tailor-Made Polymers: Via Immobilization of Alpha-Olefin Polymerization Catalysts; Severn, J. R., Chadwick, J. C., Eds.; Wiley-VHC Verlag GmbH & Co. KGaA: Weinheim, 2008; pp 1–543.
- (205) Forte, M. C.; Coutinho, F. M. B. Highly Active Magnesium Chloride Supported Ziegler-Natta Catalysts with Controlled Morphology. *Eur. Polym. J.* **1996**, *32*, 223–231.
- (206) Sozzani, P.; Bracco, S.; Comotti, A.; Simonutti, R.; Camurati, I. Stoichiometric Compounds of Magnesium Dichloride with Ethanol for the Supported Ziegler-Natta Catalysis: First Recognition and Multidimensional MAS NMR Study. J. Am. Chem. Soc. 2003, 125, 12881–12893.
- (207) Sobota, P. Metal-Assembled Compounds: Precursors of Polymerization Catalysts and New Materials. *Coord. Chem. Rev.* **2004**, 248, 1047–1060.
- (208) Malizia, F.; Fait, A.; Cruciani, G. Crystal Structures of Ziegler-Natta Catalyst Supports. *Chem. Eur. J.* **2011**, *17*, 13892–13897.
- (209) Seenivasan, K.; Sommazzi, A.; Bonino, F.; Bordiga, S.; Groppo, E. Spectroscopic Investigation of Heterogeneous Ziegler-Natta Catalysts: Ti and Mg Chloride Tetrahydrofuranates, Their Interaction Compound, and the Role of the Activator. *Chem. Eur. J.* **2011**, *17*, 8648–8656.
- (210) D'Amore, M.; Thushara, K. S.; Piovano, A.; Causà, M.; Bordiga, S.; Groppo, E. Surface Investigation and Morphological Analysis of Structurally Disordered MgCl<sub>2</sub> and MgCl<sub>2</sub>/TiCl<sub>4</sub> Ziegler-Natta Catalysts. *ACS Catal.* **2016**, *6*, 5786–5796.
- (211) D'Anna, V.; Norsic, S.; Gajan, D.; Sanders, K.; Pell, A. J.; Lesage, A.; Monteil, V.; Copéret, C.; Pintacuda, G.; Sautet, P. Structural Characterization of the EtOH-TiCl<sub>4</sub>-MgCl<sub>2</sub> Ziegler-Natta Precatalyst. *J. Phys. Chem. C* **2016**, *120*, 18075–18087.
- (212) Galli, P.; Luciani, L.; Cecchin, G. Advances in the Polymerization of Polyolefins with Coordination Catalysts. *Angew. Makromol. Chem.* **1981**, *94*, 63–89.
- (213) Huang, R.; Malizia, F.; Pennini, G.; Koning, C. E.; Chadwick, J. C. Effects of MgCl2 Crystallographic Structure on Active Centre Formation in Immobilized Single-Centre and Ziegler-Natta Catalysts for Ethylene Polymerization. *Macromol. Rapid Commun.* **2008**, 29, 1732–1738.
- (214) Thushara, K. S.; D'Amore, M.; Piovano, A.; Bordiga, S.; Groppo, E. The Influence of Alcohols in Driving the Morphology of Magnesium Chloride Nanocrystals. *ChemCatChem* **2017**, *9*, 1782–1787.
- (215) Stukalov, D. V.; Zakharov, V. A.; Potapov, A. G.; Bukatov, G. D. Supported Ziegler-Natta Catalysts for Propylene Polymerization. Study of Surface Species Formed at Interaction of Electron Donors and  $TiCl_4$  with Activated MgCl<sub>2</sub>. *J. Catal.* **2009**, *266*, 39–49.
- (216) Potapov, A. G.; Bukatov, G. D.; Zakharov, V. A. DRIFT Study of Internal Donors in Supported Ziegler-Natta Catalysts. *J. Mol. Catal. A: Chem.* **2006**, 246, 248–254.
- (217) Brambilla, L.; Zerbi, G.; Piemontesi, F.; Nascetti, S.; Morini, G. Structure of Donor Molecule 9,9-Bis(Methoxymethyl)-Fluorene in Ziegler-Natta Catalyst by Infrared Spectroscopy and Quantum Chemical Calculation. *J. Phys. Chem. C* **2010**, *114*, 11475–11484.
- (218) Thushara, K. S.; Gnanakumar, E. S.; Mathew, R.; Jha, R. K.; Ajithkumar, T. G.; Rajamohanan, P. R.; Sarma, K.; Padmanabhan, S.; Bhaduri, S.; Gopinath, C. S. Toward an Understanding of the Molecular Level Properties of Ziegler-Natta Catalyst Support with and without the Internal Electron Donor. J. Phys. Chem. C 2011, 115, 1952–1960.
- (219) Piovano, A.; D'Amore, M.; Thushara, K. S.; Groppo, E. Spectroscopic Evidences for TiCl<sub>4</sub>/Donor Complexes on the Surface of MgCl<sub>2</sub>-Supported Ziegler-Natta Catalysts. *J. Phys. Chem. C* **2018**, 122, 5615–5626.
- (220) Blaakmeer, E. S. M.; Antinucci, G.; Van Eck, E. R. H.; Kentgens, A. P. M. Probing Interactions between Electron Donors and the Support in MgCl<sub>2</sub>-Supported Ziegler-Natta Catalysts. *J. Phys. Chem. C* 2018, 122, 17865–17881.
- (221) Grau, E.; Lesage, A.; Norsic, S.; Copéret, C.; Monteil, V.; Sautet, P. Tetrahydrofuran in TiCl<sub>4</sub>/THF/MgCl<sub>2</sub>: A Non-Innocent

- Ligand for Supported Ziegler-Natta Polymerization Catalysts. ACS Catal. 2013, 3, 52-56.
- (222) Hedden, D.; Marks, T. J. [(CH<sub>3</sub>)<sub>5</sub>C<sub>5</sub>]<sub>2</sub>Th(CH<sub>3</sub>)<sub>2</sub> Surface Chemistry and Catalysis. Direct NMR Spectroscopic Observation of Surface Alkylation and Ethylene Insertion/Polymerization on MgCl2. *I. Am. Chem. Soc.* **1988**, *110*, 1647–1649.
- (223) Chizallet, C.; Costentin, G.; Lauron-Pernot, H.; Che, M.; Bonhomme, C.; Maquet, J.; Delbecq, F.; Sautet, P. Study of the Structure of OH Groups on MgO by 1D and 2D <sup>1</sup>H MAS NMR Combined with DFT Cluster Calculations. *J. Phys. Chem. C* **2007**, 111, 18279–18287.
- (224) Chizallet, C.; Costentin, G.; Che, M.; Delbecq, F.; Sautet, P. Infrared Characterization of Hydroxyl Groups on MgO: A Periodic and Cluster Density Functional Theory Study. *J. Am. Chem. Soc.* **2007**, 129, 6442–6452.
- (225) Knözinger, E.; Jacob, K. H.; Singh, S.; Hofmann, P. Hydroxyl Groups as IR Active Surface Probes on MgO Crystallites. *Surf. Sci.* **1993**, 290, 388–402.
- (226) Uzun, A.; Ortalan, V.; Browning, N. D.; Gates, B. C. Site-Isolated Iridium Complexes on MgO Powder: Individual Ir Atoms Imaged by Scanning Transmission Electron Microscopy. *Chem. Commun.* **2009**, 4657–4659.
- (227) Uzun, A.; Ortalan, V.; Browning, N. D.; Gates, B. C. A Site-Isolated Mononuclear Iridium Complex Catalyst Supported on MgO: Characterization by Spectroscopy and Aberration-Corrected Scanning Transmission Electron Microscopy. *J. Catal.* **2010**, *269*, 318–328.
- (228) Lu, J.; Aydin, C.; Browning, N. D.; Gates, B. C. Oxide- and Zeolite-Supported Isostructural  $Ir(C_2H_4)_2$  Complexes: Molecular-Level Observations of Electronic Effects of Supports as Ligands. *Langmuir* **2012**, *28*, 12806–12815.
- (229) Yardimci, D.; Serna, P.; Gates, B. C. Tuning Catalytic Selectivity: Zeolite- and Magnesium Oxide-Supported Molecular Rhodium Catalysts for Hydrogenation of 1,3-Butadiene. *ACS Catal.* **2012**, *2*, 2100–2113.
- (230) Yang, D.; Zhang, S.; Xu, P.; Browning, N. D.; Dixon, D. A.; Gates, B. C. Single-Site Osmium Catalysts on MgO: Reactivity and Catalysis of CO Oxidation. *Chem. Eur. J.* **2017**, *23*, 2532–2536.
- (231) Guzman, J.; Gates, B. C. Structure and Reactivity of a Mononuclear Gold-Complex Catalyst Supported on Magnesium Oxide. *Angew. Chem., Int. Ed.* **2003**, 42, 690–693.
- (232) Pucino, M.; Inoue, M.; Gordon, C. P.; Schowner, R.; Stöhr, L.; Sen, S.; Hegedüs, C.; Robé, E.; Tóth, F.; Buchmeiser, M. R.; Copéret, C. Promoting Terminal Olefin Metathesis with a Supported Cationic Molybdenum Imido Alkylidene N-Heterocyclic Carbene Catalyst. *Angew. Chem., Int. Ed.* **2018**, *57*, 14566–14569.
- (233) Xi, Z.; Bazzi, H. S.; Gladysz, J. A. Activation of Single-Component Nickel(II) Polyethylene Catalysts via Phase Transfer of Fluorous Phosphine Ligands. J. Am. Chem. Soc. 2015, 137, 10930–10933
- (234) Lauterwasser, F.; Hayes, P. G.; Bräse, S.; Piers, W. E.; Schafer, L. L. Scandium-Catalyzed Intramolecular Hydroamination. Development of a Highly Active Cationic Catalyst. *Organometallics* **2004**, 23, 2234–2237.
- (235) Sadow, A. D.; Tilley, T. D. Enhanced Reactivity of Cationic Hafnocene Complexes toward  $\sigma$ -Bond Metathesis Reactions. Si-H and Si-C Bond Activations in Stoichiometric and Catalytic Organosilane Conversions. *Organometallics* **2003**, *22*, 3577–3585.
- (236) Hashmi, A. S. K. Gold-Catalyzed Organic Reactions. *Chem. Rev.* **2007**, *107*, 3180–3211.
- (237) Krahl, T.; Kemnitz, E. Aluminium Fluoride-the Strongest Solid Lewis Acid: Structure and Reactivity. *Catal. Sci. Technol.* **2017**, 7, 773–796.
- (238) Yin, W.-J.; Weng, B.; Ge, J.; Sun, Q.; Li, Z.; Yan, Y. Oxide Perovskites, Double Perovskites and Derivatives for Electrocatalysis, Photocatalysis, and Photovoltaics. *Energy Environ. Sci.* **2019**, *12*, 442–462
- (239) Xia, Z.; Poeppelmeier, K. R. Chemistry-Inspired Adaptable Framework Structures. Acc. Chem. Res. 2017, 50, 1222–1230.

(240) Copéret, C.; Estes, D. P.; Larmier, K.; Searles, K. Isolated Surface Hydrides: Formation, Structure, and Reactivity. *Chem. Rev.* **2016**, *116*, 8463–8505.